Journal of Asian Earth Sciences 60 (2012) 31–48

Contents lists available at SciVerse ScienceDirect

Journal of Asian Earth Sciences

journal homepage: www.elsevier.com/locate/jseaes

Zircon U–Pb and molybdenite Re–Os geochronology and Sr–Nd–Pb–Hf isotopic constraints on the genesis of the Xuejiping porphyry copper deposit in Zhongdian, Northwest Yunnan, China

Cheng-Biao Leng [a], Xing-Chun Zhang [a,*], Rui-Zhong Hu [a], Shou-Xu Wang [b], Hong Zhong [a], Wai-Quan Wang [c], Xian-Wu Bi [a]

[a] State Key Laboratory of Ore Deposit Geochemistry, Institute of Geochemistry, Chinese Academy of Sciences, Guiyang, Guizhou 550002, China
[b] Shandong Gold Group Co. Ltd., Jinan 250014, China
[c] Branch of Mineral Resources Investigation, Yunnan Geological Survey, Kunming 650216, China

ARTICLE INFO

Article history:
Received 7 February 2012
Received in revised form 7 July 2012
Accepted 31 July 2012
Available online 16 August 2012

Keywords:
Xuejiping porphyry copper deposit
Zircon U–Pb and molybdenite Re–Os geochronology
In-situ Hf isotope
Sr–Nd–Pb isotopes
Northwest Yunnan

ABSTRACT

The Xuejiping porphyry copper deposit is located in northwestern Yunnan Province, China. Tectonically, it lies in the southern part of the Triassic Yidun island arc. The copper mineralization is mainly hosted in quartz-dioritic and quartz-monzonitic porphyries which intruded into clastic-volcanic rocks of the Late Triassic Tumugou Formation. There are several alteration zones including potassic, strong silicific and phyllic, argillic, and propylitic alteration zones from inner to outer of the mineralized porphyry bodies.

The ages of ore-bearing quartz-monzonitic porphyry and its host andesite are obtained by using the zircon SIMS U–Pb dating method, with results of 218.3 ± 1.6 Ma (MSWD = 0.31, N = 15) and 218.5 ± 1.6 Ma (MSWD = 0.91, N = 16), respectively. Meanwhile, the molybdenite Re–Os dating yields a Re–Os isochronal age of 221.4 ± 2.3 Ma (MSWD = 0.54, N = 5) and a weighted mean age of 219.9 ± 0.7 Ma (MSWD = 0.88). They are quite in accordance with the zircon U–Pb ages within errors. Furthermore, all of them are contemporary with the timing of the Garzê-Litang oceanic crust subduction in the Yidun arc. Therefore, the Xuejiping deposit could be formed in a continental margin setting.

There are negative $\varepsilon_{Nd}(t)$ values ranging from −3.8 to −2.1 and relatively high initial $^{87}Sr/^{86}Sr$ ratios from 0.7051 to 0.7059 for the Xuejiping porphyries and host andesites. The $(^{206}Pb/^{204}Pb)_t$, $(^{207}Pb/^{204}Pb)_t$ and $(^{208}Pb/^{204}Pb)_t$ values of the Xuejiping porphyries and host andesites vary from 17.899 to 18.654, from 15.529 to 15.626, and from 37.864 to 38.52, respectively, indicative of high radiogenic Pb isotopic features. In situ Hf isotopic analyses on zircons by using LA-MC-ICP-MS exhibit that there are quite uniform and slightly positive $\varepsilon_{Hf}(t)$ values ranging from −0.2 to +3.2 (mostly between 0 and +2), corresponding to relatively young single-stage Hf model ages from 735 Ma to 871 Ma. These isotopic features suggest that the primary magmas of the Xuejiping porphyries and their host andesites were mainly derived from a metasomatized mantle, with contamination of about 5–10% crustal rocks during ascending.

Comparing with typical porphyry Cu deposits, the Xuejiping porphyry Cu deposit is distinct by strong silicific and phyllic alteration and major stockwork veining mineralization in the ore-bearing porphyries, but lack of pervasive potassic alteration and disseminated mineralization. This indicates that there could be more prospective Cu resources in the Xuejiping ore district.

1. Introduction

Most porphyry-type deposits including giant deposits mainly occur in continental margin and island-arc settings (Sillitoe, 1972; Corbett and Leach, 1998; Richards, 2003), although recent studies indicate that porphyry Cu (–Mo–Au) deposits are also related to continent–continent collision (e.g., Tibet; Hou et al., 2009). The NNW-striking Zhongdian arc is the southern part of the Yidun island arc in the Sanjiang Tethyan metallogenic domain, southwestern China (Fig. 1), with an area of about 1000 km^2. Exploration activities in the Pulang, Zhuoma, Langdu, Lannitang, and Chundu prospects in the past decade suggests that the Zhongdian region would be a large prospective for porphyry Cu (Au) resources (Ren et al., 2001; Li WC et al., 2011). To date, more than ten polymetallic deposits of middle to large scales have been discovered in the Zhongdian region (Table 1), and they are dominated by Cu with estimated resources of more than 10 million tonnes of contained copper (Li WC et al., 2011). The Xuejiping porphyry

* Corresponding author. Tel.: +86 851 5895047; fax: +86 851 5891664.
E-mail addresses: lcb8207@163.com (C.-B. Leng), zhangxingchun@vip.gyig.ac.cn (X.-C. Zhang).

1367-9120/$ - see front matter © 2012 Elsevier Ltd. All rights reserved.
http://dx.doi.org/10.1016/j.jseaes.2012.07.019

Cu deposit was discovered by Team 3 of the Yunnan Bureau of Geology and Mineral Resources in 1977. There are 287,000 tonnes of contained Cu and 3 tonnes of contained Au with average grade of 0.53% for Cu and 0.06 g/t for Au.

Studies on geochronology, hydrothermal alteration, stable isotopes and fluid inclusion have been carried out for many deposits in the Zhongdian region (e.g., Zeng et al., 2003, 2004, 2006; Tan et al., 2005; Fan and Li, 2006; Lin et al., 2006; Xu et al., 2006; Wang et al., 2007a,b, 2008a,b; Leng et al., 2008a,b,c; Li WC et al., 2011; Wang et al., 2011). However, it is uncertain for the origin of the Xuejiping deposit because of relatively few detailed studies preceded (e.g., Zhong, 1982; Zhao, 1995; Zeng et al., 2003; Lin et al., 2006; Hou et al., 2007; Leng et al., 2008b, 2008c; Cao et al., 2009). In addition, several previous dating results, including a biotite Rb–Sr isochronal age of 224.6 Ma by Tan et al. (1985), an hornblende ^{40}Ar–^{39}Ar plateau age of 249.3 ± 5.0 Ma by Zeng et al. (2003), and zircon SHRIMP U–Pb dating ages of 215.3 ± 2.3 Ma by Lin et al. (2006) and 215.2 ± 1.9 Ma by Cao et al. (2009), respectively, on the quartz diorite porphyry are more or less ambiguous, because the zircon U–Pb age should be generally older than the hornblende ^{40}Ar–^{39}Ar plateau age due to the closure temperature of zircon U–Pb system (>900 °C) is higher than that of hornblende Ar–Ar system (~550 °C) (Rollinson, 1993). Moreover, the age of mineralization has not determined yet.

In this paper, a detailed description both on geological relationship and mineral paragenesis of alteration and mineralization of the Xuejiping deposit will be given. Some new results of molybdenite Re–Os and zircon U–Pb geochronological data will be presented to constrain the timing of the mineralization, the ore-bearing porphyries and their host andesites, respectively. In situ zircon Hf isotopic analysis and whole-rock Sr–Nd–Pb isotopic compositions, as well as stable isotopic compositions compiled from previous studies, will be used to discuss possible source of magma and ore-forming fluids associated with the Xuejiping porphyry copper mineralization. Implications for tectonic setting and exploration in the Zhongdian region and the Xuejiping deposit will also be briefly discussed.

2. Regional geology

The Yidun arc lies between the Songpan-Garzê Fold Belt and the Qiangtang Block of the eastern Tibetan Plateau (Yin and Harrison, 2000; Reid et al., 2005, 2007) (Fig. 1). To the east, it is bounded by the Garzê-Litang suture, which is considered to be a west-

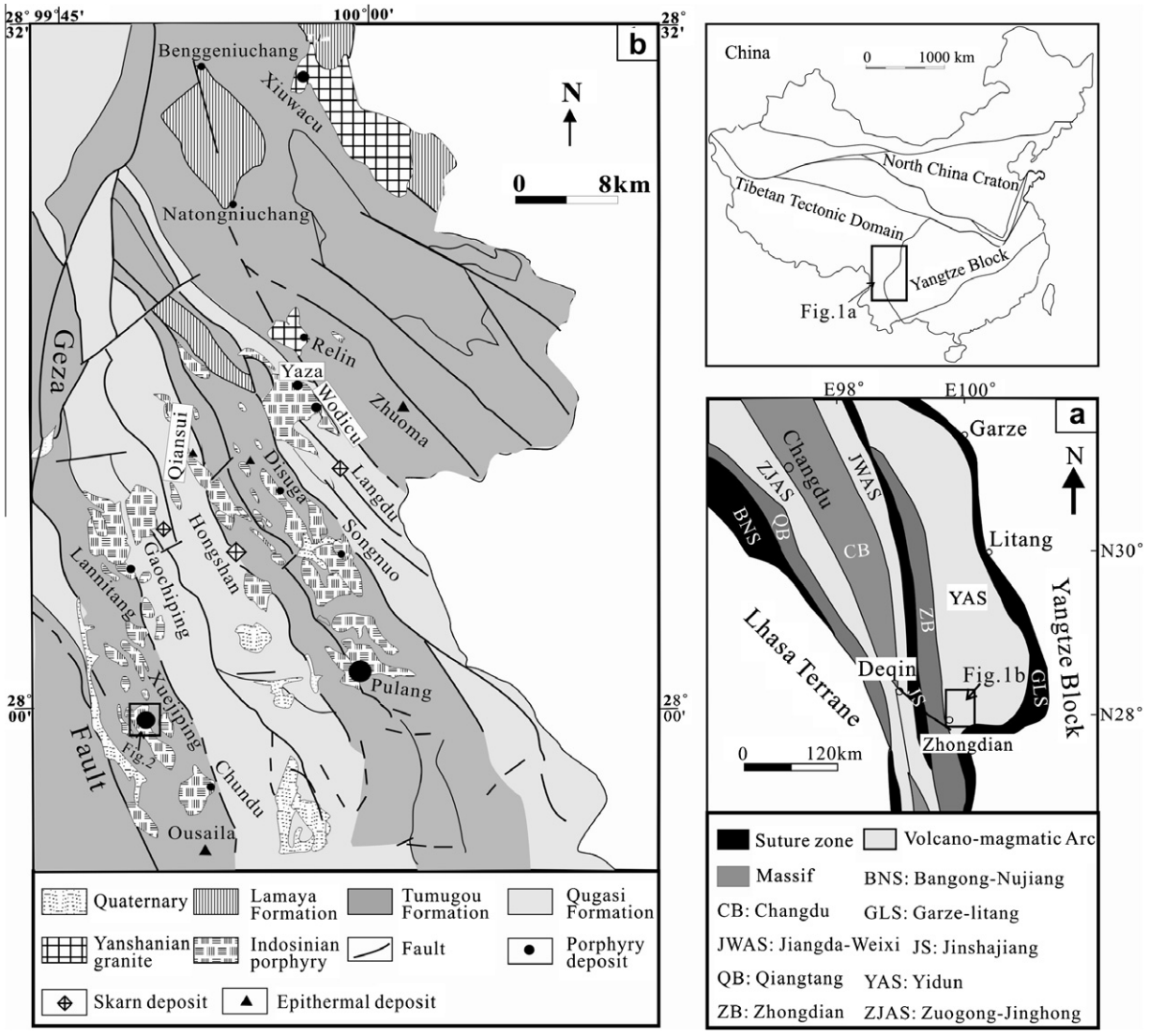

Fig. 1. (a) Tectonic framework of the Northern part of Sanjiang Tethyan Domain (modified from Mo et al. (1993) and Hou et al. (2007)) and (b) the sketch geological map of the Zhongdian island arc belt (modified from Hou et al. (2007) and Leng et al. (2007)).

Table 1
Geological features of several ore deposits and mineral occurrences in the Zhongdian area.

Deposit	Type of deposit	Metals	Resources and grade	Hosting rocks	Alteration	Ore minerals	Ages (Ma)	Reference
Pulang	Porphyry	Cu–Au	803.85 Mt@ 0.52% Cu, 0.18 g/t Au	Quartz diorite porphyry, quartz monzonite porphyry, granodiorite	Outwards from center: silicic zone → potassic zone → phyllic zone → propylitic zone	Chalcopyrite, bornite, molybdenite, covellite, pyrrhotite, pyrite, galena, sphalerite	Zircon U–Pb ages of hosting porphyry:226 ± 3–228 ± 3 Ma; Molybdenite Re–Os ages: 213 ± 3.8 Ma; 218 ± 3.4–219.7 ± 3.4 Ma	Wang et al. (2008a,b), Zeng et al.(2006), Cao (2007), Li WC et al.(2011)
Xuejiping	Porphyry	Cu	54.15 Mt @ 0.53%Cu, 0.06 g/t Au	Quartz diorite porphyry, quartz monzonite porphyry	Outwards from center: potassic alteration → silic–phllic alteration → argillization → propylitization	Chalcopyrite, pyrite, galena, sphalerite	Zircon U–Pb ages of hosting porphyry: 215.3 ± 2.3–218.4 ± 1.7 Ma; Molybdenite Re–Os ages: 221.4 ± 2.3 Ma	This study, Lin et al. (2006) and Cao et al. (2009)
Lannitang	Porphyry	Cu–Au	36 Mt @0.50% Cu, 0.45 g/t Au	Diorite porphyry, quartz diorite porphyry, quartz monzonite porphyry	Silicification, gypsification, phyllic, chloritization, carbonization, arigllization	Chalcopyrite, pyrite, bluechalcocite, cuprite, magnetite, hematite	Zircon U–Pb ages of hosting porphyry: 219.2 ± 1.8 Ma	Our unpublished data
Chundu	Porphyry	Cu	No data	Diorite porphyry, granodiorite porphyry	Potassic alteration, Silicification, phyllic, propylitization	Chalcopyrite, pyrite, galena, sphalerite	Zircon U–Pb ages of hosting porphyry: 219.7 ± 1.8 Ma	Our unpublished data
Songnuo	Porphyry	Cu	No data	Quartz diorite porphyry, biotite quartz monzonite porphyry, diorite porphyry, quartz monzonite porphyry	Silicification, chloritization, carbonization	Chalcopyrite, bornite, pyrite, magnetite, galena	Zircon U–Pb ages of hosting quartz monzonite porphyry: 220.9 ± 3.5 Ma	Ren et al. (2001) and Leng et al. (2008a,b,c)
Disuga	Porphyry	Cu	No data	quartz diorite porphyry, quartz monzonite porphyry	Phyllic, slicification, chloritization	Chalcopyrite, bornite, sphalerite, pyrite, galena	Zircon U–Pb ages of hosting quartz monzonite porphyry: 231.0 ± 5.1 Ma	Our unpublished data
Hongshan	Skarn	Cu–polymetellic	23.76 Mt @ 1.01% Cu, 4.87% Pb, 4.86% Zn	Cu mineralization in skarn; Mo mineralization in monzonite granite porphyry	Skarnization	Chalcopyrite, molybdenite, pyrite, galena, sphalerite	Rb–Sr isochronal age of hosting porphyry: 214 Ma Molybdenite Re–Os age: 77 ± 2 Ma	YBGMR (1990) and Xu et al. (2006)
Langdu	Skarn	Cu	1.67 Mt @ 6% Cu	SKARN	Skarnization, marmarization, carbonatization	Chalcopyrite, pyrrhotite, pyrite	Biotite ^{39}Ar–^{40}Ar age of monzonite granite: 216.93 ± 4.34 Ma	Zeng et al. (2003)
Gaochiping	Skarn	Cu	No data	Skarn, diorite porphyry	Skarnization, Silicification, chloritization,	Chalcopyrite, pyrite, bornite	No date	Ren et al. (2001)
Zhuoma	Epithermal	Cu–polymetallic	No data	Diorite porphyry, skarn	Phyllic, skarnization	Chalcopyrite, pyrite, sphalerite, galena	No date	Ren et al. (2001)
Xiuwacu	Hydrothermal	W–Mo	No data	Monzonite granite Biotite monzogranite	Potassic alteration Silicification greisenization arigllization	Scheelite,molybdenite, pyrite,Chalcopyrite	Rb–Sr isochronal age of monzonite granite:88.3 Ma Molybdenite Re–Os age: 81 ± 3 Ma	Hou et al. (2003) and Li et al. (2007)
Relin	Hydrothermal	W–Mo–Cu	No data	Monzonite granite Biotite monzogranite	Silicification greisenization arigllization	Scheelite,molybdenite, Chalcopyrite, cassiterite, pyrite	Biotite ^{39}Ar–^{40}Ar age of monzonite granite: 82.0 ± 0.8 Ma Molybdenite Re–Os age: 81.2 ± 2.3 Ma	Yin et al. (2009) and Li et al. (2007)

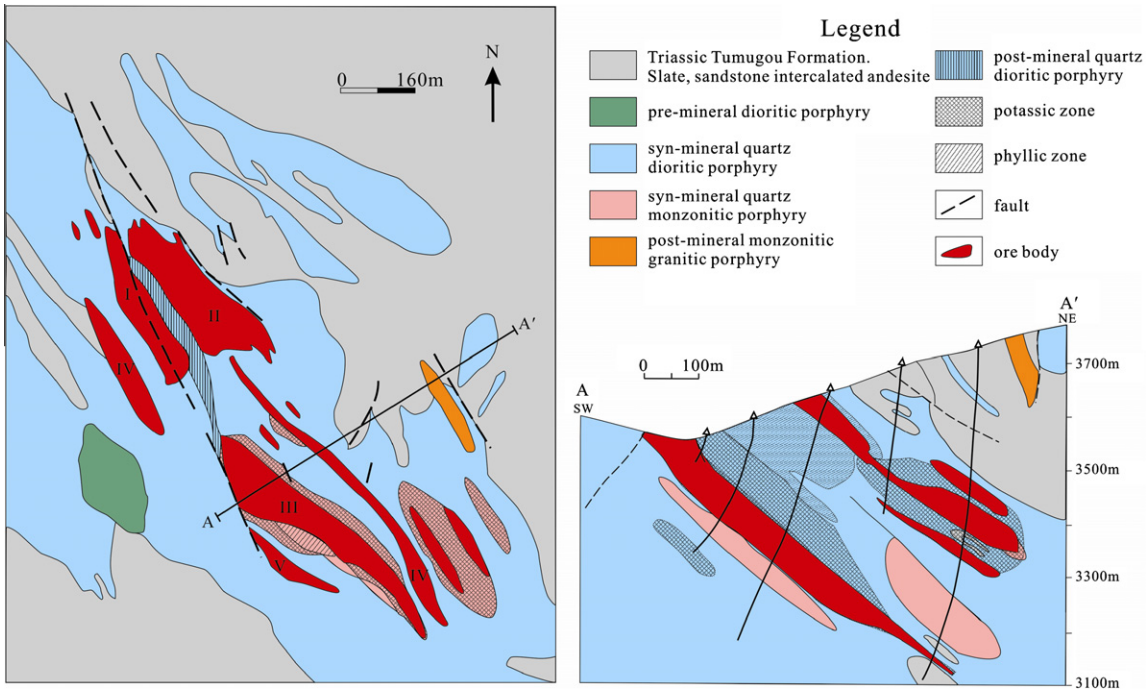

Fig. 2. Simplified geological map and cross-section of the Xuejiping porphyry Cu deposit (modified from Huang et al. (2001) and Hou et al. (2003)).

ward-dipping Paleo-Tethys oceanic subduction zone during the Middle–Late Triassic (Zhong, 2000). To the west, it is bounded by the Jinshajiang suture which is considered to be a Late Paleozoic Paleo-Tethys oceanic subduction zone dipping to the west (Sengör, 1985; Chen et al., 1987; Li et al., 1999; Wang et al., 2000; Zhong, 2000) or to the east (Reid et al., 2005). Therefore, the Yidun arc is an important tectonic unit of the Tethy-Himalayan orogenic belts. Meanwhile, it is also a significant Cu–Ag–Sn polymetallic mineralization belt in the Sanjiang Tethyan metallogenic domain (Qu et al., 2002; Pan et al., 2003; Hou et al., 2003, 2007; Li WC et al., 2011).

The oldest rocks currently exposed in the Yidun arc are Paleozoic metasedimentary rocks in the Zhongza Massif (Fig. 1; e.g. Chang, 1997), or called as "western Yidun arc" by Reid et al. (2005). These carbonate-rich Palaeozoic successions have fossil assemblages similar to sediments and metasediments of the Longman Shan Thrust Nappe Belt, west of the Yangtze Block (Chang, 1997). Therefore, it is thought that the Zhongza Massif was separated from the Yangtze Block due to the opening of the Garzê-Litang Ocean during the middle to late Palaeozoic, possibly associated with a major Permian phase regional extension (Zhang et al., 1998). The Palaeozoic metasediments of the Zhongza Massif were separated from the Triassic cover sequences of the Qiangtang Block to the west by the Jinshajiang Suture (Fig. 1), which is interpreted to have closed in the Middle Triassic (e.g., Wang et al., 2000; Zhong, 2000). Triassic sequences of clastic rocks intercalated with arc volcanic rocks overlie on the Palaeozoic sequences of the Yidun arc. The arc volcanic rocks were formed during the westward-dipping subduction of the so-called "Garzê-Litang Ocean" during the Late Triassic (Chen et al., 1987; Hou and Mo, 1991; Hou, 1993). Jurassic and Cretaceous sediments are absent in the Yidun arc, although there is a belt of Cretaceous granites in the eastern Yidun arc (Qu et al., 2002; Reid et al., 2007). In addition, voluminous granite and granodiorite plutonic batholiths intruded into the deformed Paleozoic and Triassic volcanic–sedimentary rocks across the arc. These granites were emplaced in four episodes (206–238 Ma, 138–206 Ma, 76–135 Ma and 65–15 Ma) (Hou et al., 2001). The Yidun arc was deformed during the Indosinian orogeny which resulted from the terminal accretion of the Qiangtang Block to the southern margin of Eurasia during the Late Triassic to Jurassic (e.g., Xu et al., 1992; Burchfiel et al., 1995; Zhou and Graham, 1996; Harrowfield and Wilson, 2005; Reid et al., 2005, 2007). Following the collision of India with Asia during the Tertiary, the Yidun arc was incorporated into the modern Tibetan Plateau and deformed by numerous strike–slip faults and localized zones of transpression (Ratschbacher et al., 1996; Wang and Burchfiel, 2000; Reid et al., 2005).

In the northern Yidun arc (the "Changtai" arc), widely distributed Late Triassic bimodal volcanic suites and arc-type volcanic rocks host numerous sulfide deposits (Hou et al., 2003), including the large Gacun Ag-polymetallic VMS deposit (Hou and Mo, 1993; Hou et al., 2001). In the southern Yidun arc (the "Zhongdian" arc), numerous Late Triassic intermediate-felsic porphyry bodies which intruded into contemporaneous volcanic–sedimentary rocks contain porphyry-type or skarn-type Cu-polymetallic mineralization. These porphyries can be roughly classified into the East and West porphyry belts, separated by the Geza River (YBGMR, 1990; Zeng et al., 2003; Li WC et al., 2011). The East porphyry belt mainly comprises the Pulang, Songnuo, Langdu and Qiansui hypabyssal intrusive complexes (Fig. 1b). The West porphyry belt comprises the Lannitang, Xuejiping, Chundu and Ousaila hypabyssal intrusive complexes (Fig. 1b).

3. Deposit geology

The Xuejiping porphyry Cu deposit is located at 99°50′15″E and 28°02′N, 25 km northeast of the Shangri-la (Zhongdian) County town. It is the first porphyry Cu deposit discovered in the Zhongdian area. It is situated in the center of the West porphyry belt. The newly discovered Lannitang and Chundu porphyry Cu deposits are located in its north and south sides, respectively (Fig. 1b).

3.1. Local stratigraphy and structural geology

The main exposed strata (Fig. 2) in the Xuejiping area comprise the Upper Triassic Tumugou Formation which conformably over-

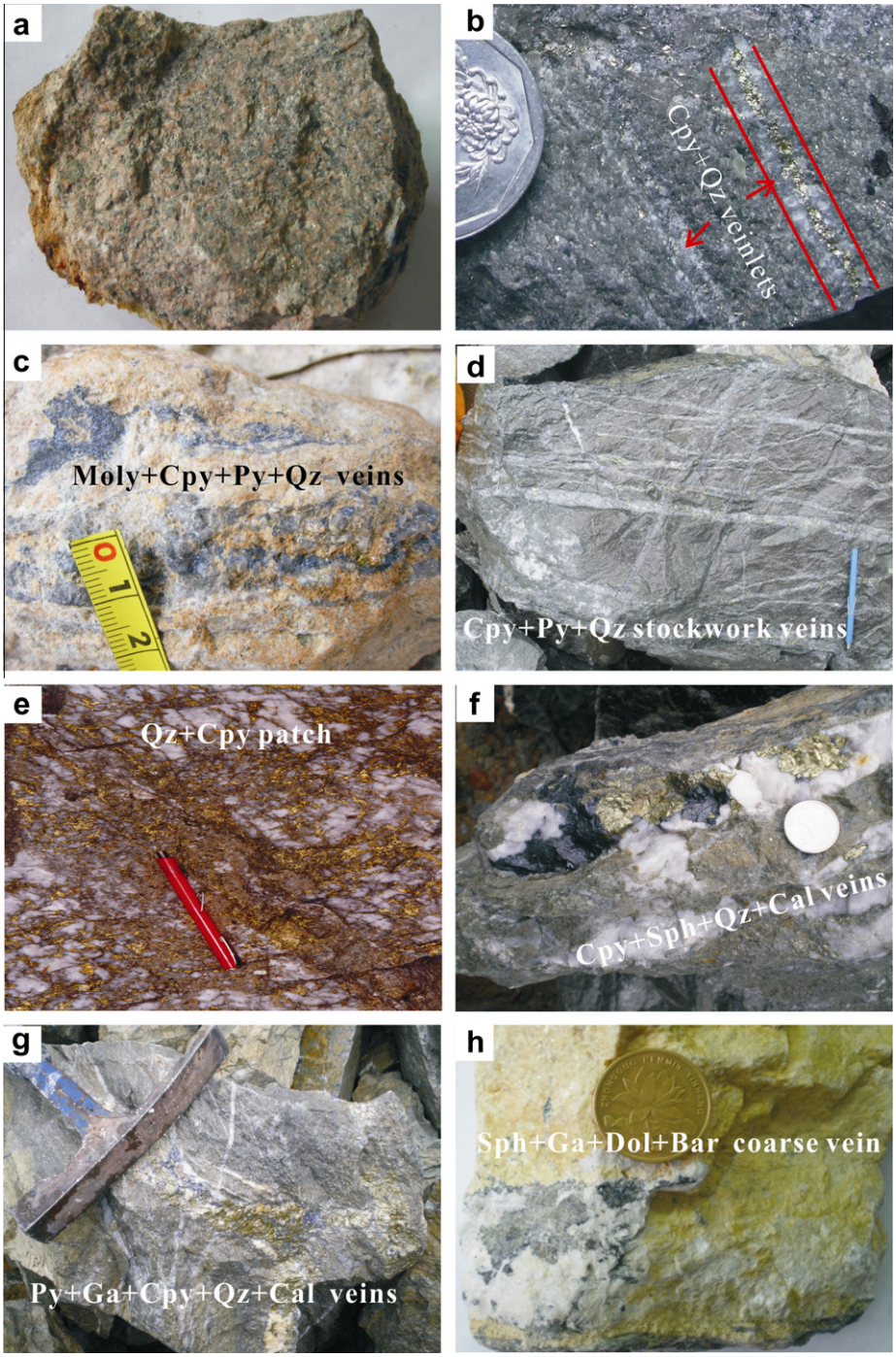

Fig. 3. Macro-photographs of ores. (a) potassic altered quartz monzonitic porphyry; (b) quartz–chalcopyrite veinlets in the quartz dioritic porphyry; (c) quartz–molybdenite–chalcopyrite–pyrite in the quartz monzonitic porphyry; (d) quartz–chalcopyrite–pyrite stockwork veins in quartz diorite porphyry; (e) quartz–chalcopyrite patches in strong silicic and phyllic zones; (f) chalcopyrite–sphalerite–quartz–calcite veins; (g) pyrite–galena–sphalerite–chalcopyrite–calcite–quartz veins; (h) sphalerite–galena–dolomite–barite coarse vein. Abbreviations of minerals: Bar – barite, Cal – calcite, Cpy – chalcopyrite, Dol – dolomite, Ga – galena, Moly – molybdenite, Py – pyrite, Qz – quartz, Sph – sphalerite.

lies the Upper Triassic Qugasi Formation (YBGMR, 1990; Li, 2007). The Tumugou Formation is composed of three members from bottom to top (Li, 2007). Member 1 is composed mainly of dark gray slates and meta-sandstone, with locally thin layers of limestone and conglomerate. Its thickness varies from 488 m to 634 m. Member 2 is composed mainly of dark gray slate, sandy sericite slate, and intermediate to intermediate-felsic volcanic rocks. Its thickness varies from 2347 m to 2713 m. It hosts the Cu mineralized porphyry bodies. Member 3 consists dominantly of dark gray slates and sandy sericite slate, with meta-sandstone and crystalline limestone. Its thickness is more than 270 m.

There are abundant bivalve fossils in the Tumugou Formation, implying that it is a deep-water flysch–volcanic formation, similar to continental margin turbidite sedimentation (Li, 2007).

Faults are well developed in the Xuejiping area and are controlled by the activity of the Geza deep fracture (Fig. 2). There are about 15 major faults in the deposit area. They are characterized by high-angle strike–slip thrust faults with predominant

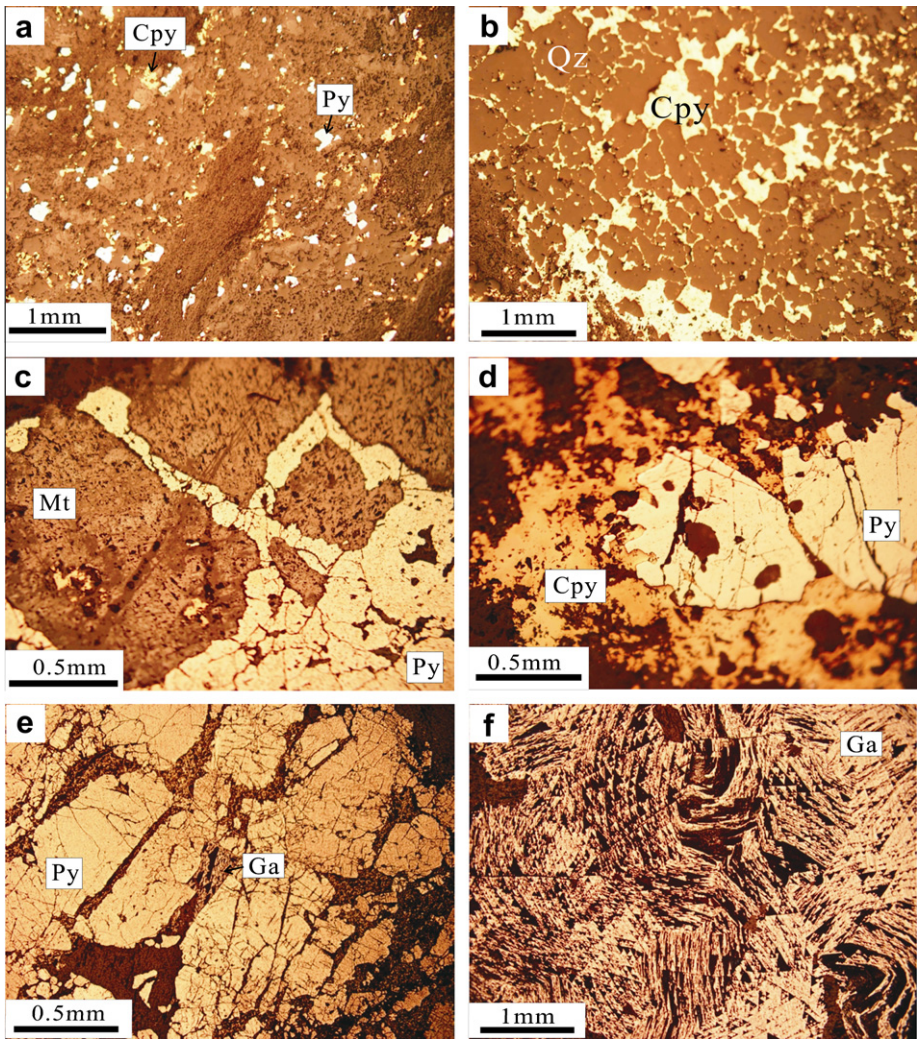

Fig. 4. Reflected light photomicrographs of various ore. (a) pyrite and chalcopyrite dissemination in the potassic quartz monzonite porphyry (Fig. 3a); (b) chalcopyrite is interstitial with quartz grains (Fig. 3e); (c) pyrite crosscutting magnetite; (d) early pyrite is cut and replaced by late chalcopyrite; (e) galena crosscutting pyrite; (f) crumpled structure of galena formed under stress. Abbreviations of minerals: Cpy – chalcopyrite, Ga – galena, Mt – magnetite, Py – pyrite, Qz – quartz.

NNW- and NE-striking and the dip angles varying from 50° to 70° (Fig. 2). These strike–slip thrust faults probably resulted in some local dilation zones as pathway channels for magma and hydrothermal fluids (Zhong, 1982). The copper mineralization is controlled by small fractures in porphyry bodies. According to the drill core logging, there are more than eight fractures in each 10 cm-long core of mineralized porphyry, whereas only 2–3 fractures are presented in each 10 cm-long core of barren porphyry (Zhong, 1982; Hou et al., 2003).

3.2. The Xuejiping intrusive complex

The Xuejiping complex is composed of more than 20 hypabyssal porphyries with an area of about 2 km^2. It intruded into Member 2 of the Tumugou Formation with approximately NNW-direction extension along faults and strata in this area (Fig. 2). Detailed field observations indicate that the Xuejiping complex can be divided into two intrusive clusters (Zhong, 1982). The early cluster consists of pre-mineral diorite porphyry, syn-mineral quartz diorite porphyry and quartz monzonite porphyry. The late cluster consists of post-mineral monzonitic granite porphyry and granite porphyry. The most widely distributed porphyry in the Xuejiping deposit area is quartz diorite porphyry which covers an area of about 0.94 km^2 with NNW-trending length of 2.4 km and width of 0.5–0.78 km (Fig. 2).

The pre-mineral diorite porphyry usually occurs as dike and accompanies eruption of andesite. It is grayish green, with massive structure and porphyritic texture. It is composed of phenocrysts of plagioclase (23–40%), amphibole (10–25%) and biotite (1–5%) and fine to microgranular sized groundmass of plagioclase, chlorite and minor quartz, with minor accessory minerals of zircon, apatite and rutile. Alteration is dominated by chloritization, sericitization and silicification.

The syn-mineral quartz diorite porphyry is gray, with massive structure and porphyritic–blastoporphyritic texture. It is composed of phenocrysts of plagioclase (20–45%), muscovite (0–8%), biotite (0–10%), amphibole (0–10%) and quartz (0–5%), and fine to mircogranular sized matrix of plagioclase, K-feldspar and quartz, with minor accessory minerals of zircon, apatite, magnetite and rutile. The plagioclase phenocrysts generally occur as 1–4 mm sized euhedral tabular crystals with well-developed polysynthetic twin and rhythmic zonation. Most of plagioclase grains are altered to sericite–quartz–clay, while dark minerals are generally altered to chlorite.

The syn-mineral quartz monzonite porphyry is pinkish gray with porphyritic texture and massive structure. It is composed of

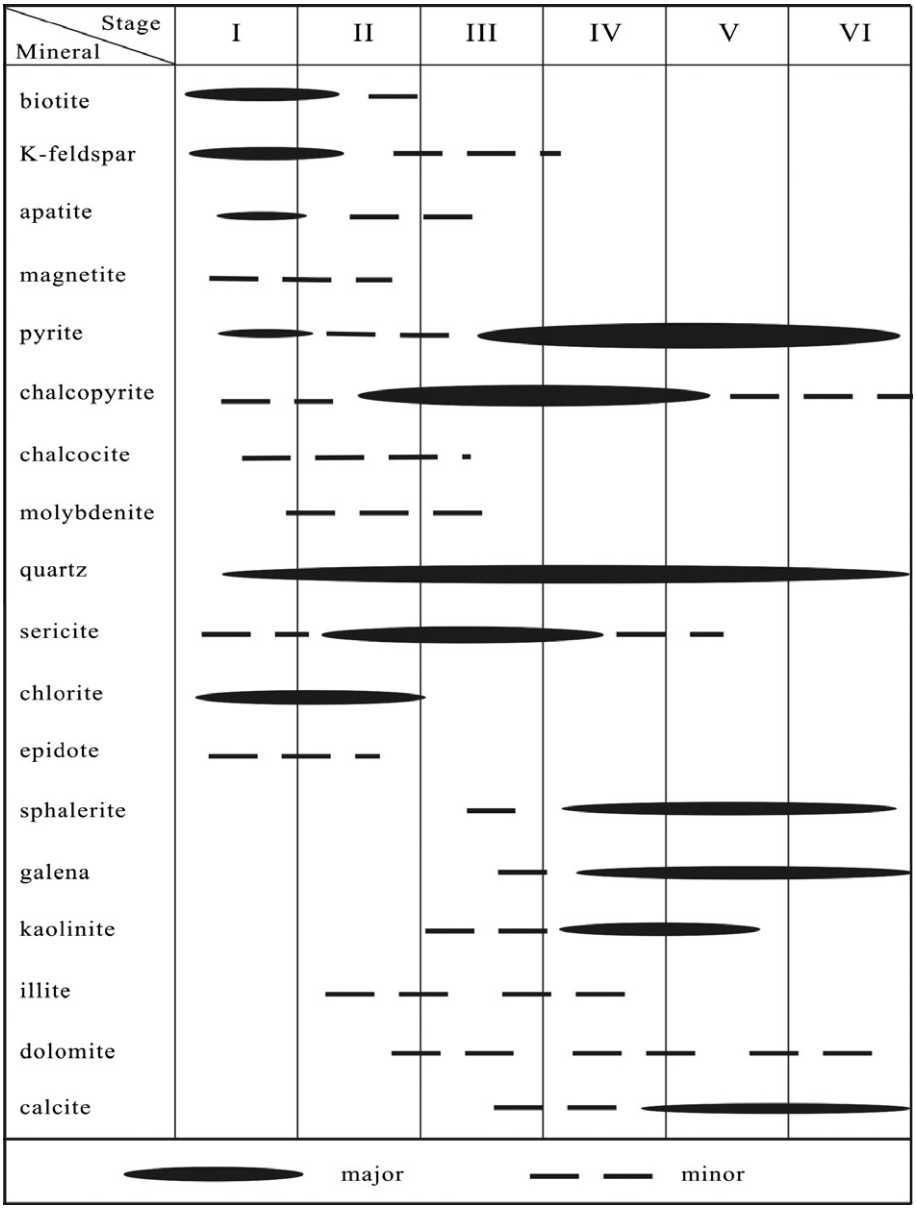

Fig. 5. Simplified paragenetic sequence of ore and gangue minerals from the Xuejiping porphyry Cu deposit and related stages of Cu mineralization.

phenocrysts of plagioclase (20–30%), K-feldspar (5–15%), biotite (0–5%) and amphibole (0–5%), and fine to mircogranular sized matrix of the K-feldspar and quartz, with minor accessory minerals of zircon, apatite and rutile. Alteration is dominated by sericitization, K-feldsparization, silicification and pyritization.

The post-mineral quartz diorite porphyry occurs as dike and cut the Number I and Number II ore bodies (Fig. 2). It is petrologically similar to the quartz diorite porphyry of the early unit, but displays weakly phyllic alteration and mineralization.

The post-mineral monzonitic granite porphyry occurs as dike in the eastern part of the main intrusive body (Fig. 2). It is pinkish gray with porphyritic texture and massive structure. It comprises phenocrysts of plagioclase, K-feldspar, amphibole and biotite, and fine to mircogranular sized matrix of K-feldspar and quartz.

3.3. Alteration and mineralization

3.3.1. Hydrothermal alteration and zonation

In the Xuejiping deposit area, various types of hydrothermal alteration are distributed. They include potassic alteration, silicification, albitization, sericitization, pyritization, chloritization, argillization, and carbonation. The mineralized porphyry rocks show obvious alteration zones which are similar to other porphyry Cu deposits in the world (Lowell and Guilbert, 1970; Corbett and Leach, 1998). From the center to the outer parts of the mineralized porphyry body, four alteration zones have been identified. They include potassic alteration zone, strong silicic and phyllic alteration zone, argillic alteration zone, and propylitic alteration zone (Fig. 2). The Cu mineralization is closely related to the strong silicic and phyllic alteration zone.

Potassic alteration zone consists of K-feldspar, secondary biotite and quartz, and locally minor albite and magnetite. This zone is distributed in the center of the mining area and dominantly located within the syn-mineral quartz monzonite porphyry. There is abundant chalcopyrite and pyrite, and minor molybdenite which are disseminated in the quartz monzonite porphyry (Figs. 3a, b and 4a).

Strong silicic and phyllic alteration zone is distributed in the center of the syn-mineral quartz diorite porphyry, and consists dominantly of quartz, sericite and pyrite. In this zone, patches

and stockwork veins of quartz are well developed. Meanwhile, sercitization occurs pervasively in the ore-bearing porphyries. Cu mineralization is intimately associated with the strong silicification (Fig. 3d and e).

Argillic alteration zone is distributed outside of the strong silicic and phyllic alteration zone. It is characterized by sericite, which formed by the alteration of feldspar and was altered further to clay minerals (kaolinite, illite, and dickite). Limited Cu mineralization occurred in this zone (Fig. 3f and g).

Propylitic alteration zone is distributed outside of the argillic alteration zone and composed mainly of chlorite, carbonate, and minor epidote. It occurs very commonly and widely within the pre-mineral diorite porphyry and andesite. A few ore-bearing quartz veins have been observed in this zone.

3.3.2. Mineralization and paragenesis

The Cu mineralization zone occupies about 1/3 volume of the quartz diorite porphyry body, with a length of 1100 m and a width of 300 m (Fig. 2; Zhong, 1982). Four major NNW-trend lentoid orebodies have been delineated in the deposit. Orebody I and orebody II in the north are hosted in the altered quartz diorite porphyry, while the orebody III and orebody IV in the south are mainly hosted in the altered quartz monzonite porphyry. Orebody IV has been mainly mined at present.

There are various mineralization types including dissemination (Fig. 4a), stockwork veining (Fig. 3d) and coarse veining (Fig. 3f–h) in the deposit. There are dominant sulfides of chalcopyrite and pyrite, with minor chalcocite, cuprite, galena, sphalerite, and molybdenite in the ore (Fig. 3c). Gangue minerals include quartz, plagioclase, sericite, biotite, chlorite, epidote, kaolinite, illite, calcite, dolomite and barite. EPMA analysis show that there are trace amounts of Mo (0.18–0.53 wt.%) and As (0.41–0.90 wt.%) in pyrite, chalcopyrite and sphalerite (our unpublished data).

Based on the mineral assemblages and crosscutting relationships of various veins (Figs. 3 and 4), six stages of Cu mineralization which are accompanied by relevant types of alteration have been identified. The paragenetic sequence of metallic and gangue minerals of this deposit and their relationship to stages of mineralization are shown in Fig. 5.

Stage I of Cu mineralization is characterized by the dissemination of fine chalcopyrite, with an assemblage of chalcopyrite, pyrite, K-feldspar, and magnetite. It is associated with potassic alteration. Chalcopyrite and pyrite spots are generally disseminated in weakly potassic altered porphyry which contains little quartz veins (Fig. 4a).

Stage II of Cu mineralization is represented by the distribution of patchy chalcopyrite, with an assemblage of quartz, chalcopyrite, and pyrite. It is associated with strong silicification (Fig. 3d and e). Sulfides spots are distributed interstitially among the quartz crystals (Fig. 4b). Only minor high grade Cu ore were formed in this stage.

Stage III of Cu mineralization is characterized by the distribution of veining and stockwork veining chalcopyrite, with an assemblage of quartz, sericite, chalcopyrite, molybdenite, and pyrite (Figs. 3b, c and 4d). It is mainly associated with phyllic alteration. Major Cu mineralization occurred in this stage.

Stage IV of Cu mineralization is marked by coarse veining chalcopyrite, with an assemblage of quartz, carbonate, pyrite, chalcopyrite, and sphalerite (Fig. 3e). Minor low grade Cu ore bodies were formed in this stage.

Stage V of Cu mineralization is featured by both the veining and disseminated chalcopyrite, with an assemblage of quartz, clay, chlorite, pyrite, and chalcopyrite. It is associated with the argillic alteration overprinted on the phyillic alteration.

Stage VI of Cu mineralization is represented by the veins or stockwork veins of carbonate–quartz–pyrite–galena–sphalerite–chalcopyrite (Figs. 3g, h, 4e and f).

4. Samples and analytical methods

4.1. Molybdenite Re–Os analytical methods

Five molybdenite samples collected from Orebody IV were chosen for Re–Os isotopic dating. The molybdenite was mostly very fine grained and was distributed as a film on the walls of the potassic altered porphyries (e.g., Fig. 3c). Gravity separation method was applied firstly to separate molybdenite from the finely crushed mineralized rocks. Then molybdenite grains were handpicked individually under a binocular microscope to get over 99% purity molybdenite separates. Re–Os sample dissolution and preparation were performed at the Key Laboratory of Isotope Geochronology and Geochemistry, Guangzhou Institute of Geochemistry, Chinese Academy of Sciences. Re and Os concentration and isotopic composition were measured using a Thermo ICP-MS (TJA X-7) at the Laboratory of Mineralization and Dynamics, Chang'an University. The detailed analytical procedures were described by Sun et al. (2010) and Li N et al. (2011). Average blanks of this analysis were ca. 2.8 pg for Re and 0.7 pg for Os, respectively, which was negligible for the measured Re and Os abundances. The molybdenite model ages were calculated by using an equation of $t = [\ln(1 + {}^{187}Os/{}^{187}Re)]/\lambda$, where λ is the ^{187}Re decay constant of 1.666×10^{-11} year^{-1} (Smoliar et al. 1996). Re–Os isotopic data have been processed by using the ISOPLOT 2.49 program (Ludwig 2001).

4.2. Zircon SIMS U–Pb dating methods

In order to constrain the formation age and the origin of the porphyry, one sample of syn-mineral quartz monzonite porphyry (X07-23) and another sample of peripheral andesite (X07-20) in the Tumugou Formation have been selected for zircon U–Pb dating and in situ Lu–Hf isotopic analyses.

Firstly, zircon grains were separated respectively from about 5 kg of the X07-23 and X07-20 samples by using conventional heavy liquid and magnetic separation techniques and hand picking. Secondly, the zircon separates, together with the zircon standards Plešovice (Sláma et al., 2008) and Qinghu (Li et al., 2009) were mounted in epoxy mounts which were then polished to section the crystals in half for analyses. Thirdly, all zircon crystals of the separates and standard grains on the mounts were documented with transmitted and reflected light micrographs as well as cathodoluminescence (CL) images to reveal their external and internal structures. The micrographs were taken under the microscope at the State Key Laboratory of Ore Deposit Geochemistry (SKLODG) in Guiyang. The CL images were obtained by using a microprobe associated instrument JEOL JXA-8900RL at the Institute of Geology of the Chinese Academy of Geological Sciences in Beijing. Fourthly, the mount was vacuum-coated with high-purity gold for analyzing zircon U–Pb isotopic compositions and U, Th and Pb concentrations which were conducted by using Cameca IMS 1280 SIMS at the Institute of Geology and Geophysics, Chinese Academy of Sciences in Beijing (IGGCAS). The analytical procedures are described by Li et al. (2009). Measured compositions were corrected for common Pb by using the measured non-radiogenic ^{204}Pb. Uncertainties on individual analyses are reported at 1σ level, and weighted mean ages for pooled U–Pb analyses are quoted with 95% confidence interval. Data reduction was carried out by using the Isoplot program of Ludwig (2001).

Table 2
Re–Os data for molybdenite from the Xuejiping porphyry Cu deposit.

Sample	Weight (g)	Re (ppm)		^{187}Re (ppm)		^{187}Os (ppm)		Model age (Ma)	
		Measured	±2σ	Measured	±2σ	Measured	±2σ	Measured	±2σ
X1	0.0208	1467	2.76	922	1.74	3.40	0.032	221.0	2.1
X2	0.0148	2437	8.83	1530	5.55	5.61	0.059	220.5	2.4
X3	0.0232	997	3.47	625	2.18	2.29	0.009	219.6	1.2
X6	0.0174	1237	8.38	775	5.27	2.86	0.015	220.9	1.9
X14	0.0302	728	1.87	458	1.18	1.68	0.007	219.5	1.1

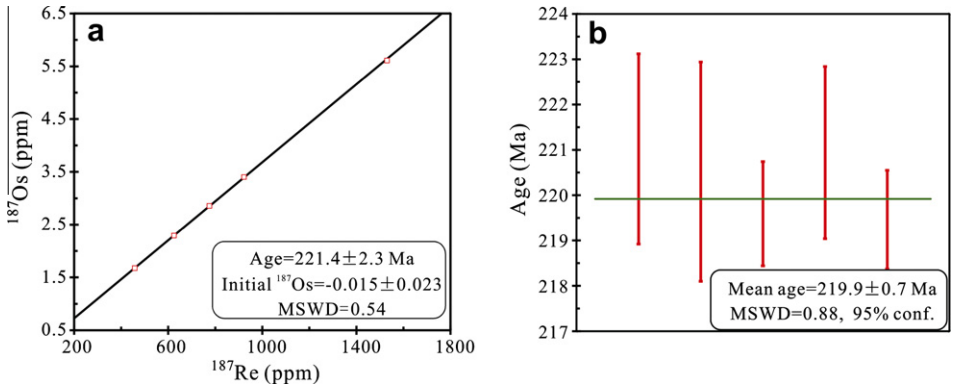

Fig. 6. Re–Os isochronal diagram (a) and weighted average model age diagram (b) for the molybdenite samples from the Xuejiping deposit.

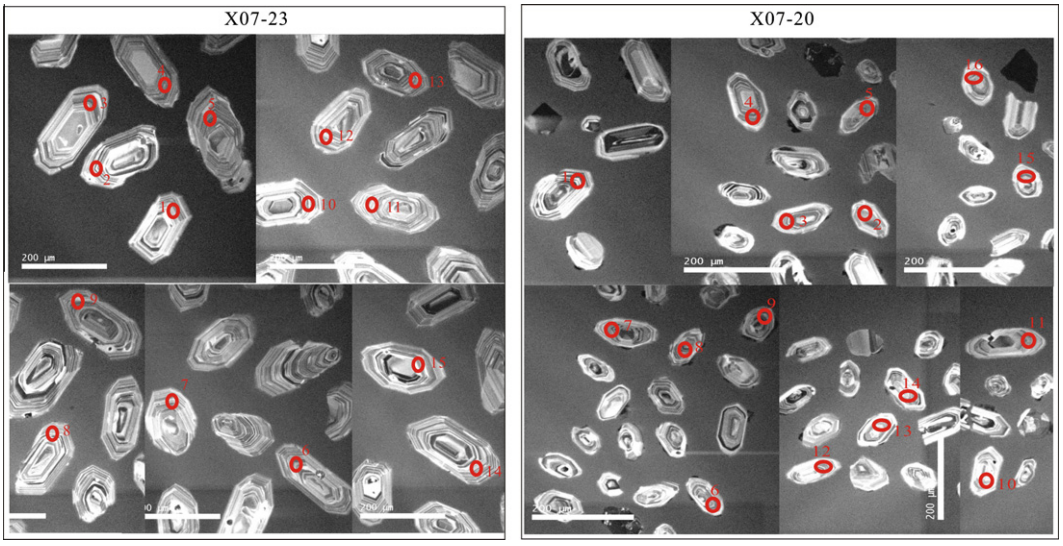

Fig. 7. Cathodoluminescence (CL) images of zircon grains from the ore-bearing quartz monzonite porphyry (X07-23) and andesite (X07-20) in the Xuejiping porphyry Cu deposit. The ellipses indicate the SIMS analysis spots for U–Pb isotopes.

4.3. In-situ zircon Hf analysis

In situ zircon Lu–Hf isotopic analysis was carried out on those zircon grains that were previously analyzed for U–Pb isotopes by using a Neptune multi-collector ICP-MS equipped with a Geolas-193 laser-ablation system at the IGGCAS. During the course of this study, a laser repetition rate of 10 Hz at 100 mJ was used and the laser beam diameters were either 40 or 60 μm. Isobaric interference of ^{176}Lu on ^{176}Hf was corrected by measuring the intensity of the interference-free ^{175}Lu isotope and using a recommended ^{176}Lu/^{175}Lu ratio of 0.02669 (De Bievre and Taylor, 1993) to calculate ^{176}Lu/^{177}Hf ratios. The ^{176}Yb/^{172}Yb value of 0.5886 (Chu et al., 2002) and mean βYb value obtained during Hf analysis on the same spot were applied for the interference correction of ^{176}Yb on ^{176}Hf (Iizuka and Hirata, 2005). Measured ^{176}Hf/^{177}Hf ratios were normalized to ^{179}Hf/^{177}Hf value of 0.7325. The detailed analytical procedures were described by Wu et al. (2006).

During the course of this study, a weighted mean ^{176}Hf/^{177}Hf ratio of the standard zircon Mud Tank of 0.282516 ± 5 (2σ) is yielded. It is in good agreement with the reported ^{176}Hf/^{177}Hf ratios of 0.282507 ± 6 (2σ) from solution analysis by Woodhead and Hergt (2005) and of 0.282523 ± 43 (2σ) from in situ analysis by Griffin et al. (2006). Initial Hf isotopic ratios are calculated with the reference to the chondritic reservoir at the time of magma crystallization that corresponds to age of zircon growth from magma. A decay constant for ^{176}Lu of 1.865×10^{-11} yr^{-1} (Scherer et al., 2001), and the chondritic ratios of 0.282772 for ^{176}Hf/^{177}Hf and 0.0332 for ^{176}Lu/^{177}Hf given by Blichert-Toft and Albarede (1997)

Table 3
SIMS zircon U–Pb data for the ore-bearing quartz monzonite porphyry and peripheral andesite from the Xuejiping porphyry Cu deposit.

Spots	U (ppm)	Th (ppm)	Th/U	$^{207}Pb/^{206}Pb$	±1σ (%)	$^{207}Pb/^{235}U$	±1σ (%)	$^{206}Pb/^{238}U$	±1σ (%)	$t_{207/235}$ (Ma)	±1σ	$t_{206/238}$ (Ma)	±1σ	f_{206} (%)
X07-23 quartz monzonite porphyry														
1	266	172	0.65	0.05088	1.55	0.24376	2.17	0.0347	1.51	221.5	4.3	220.2	3.3	0.04
2	314	265	0.84	0.05126	1.68	0.23939	2.28	0.0339	1.55	217.9	4.5	214.7	3.3	0.07
3	409	361	0.88	0.05101	1.30	0.24745	2.00	0.0352	1.51	224.5	4.0	222.9	3.3	0.05
4	391	303	0.78	0.04999	1.40	0.23669	2.06	0.0343	1.51	215.7	4.0	217.7	3.2	0.08
5	184	136	0.74	0.05083	2.49	0.24030	2.91	0.0343	1.52	218.7	5.7	217.3	3.2	0.08
6	324	226	0.70	0.04999	1.40	0.23864	2.05	0.0346	1.50	217.3	4.0	219.4	3.2	0.00
7	291	213	0.73	0.05101	1.46	0.24092	2.10	0.0343	1.51	219.2	4.2	217.1	3.2	0.03
8	416	454	1.09	0.05015	1.23	0.23780	1.95	0.0344	1.52	216.6	3.8	218.0	3.3	0.00
9	284	191	0.67	0.05208	1.46	0.24683	2.10	0.0344	1.51	224.0	4.2	217.9	3.2	0.03
10	346	294	0.85	0.05070	1.34	0.24060	2.02	0.0344	1.51	218.9	4.0	218.1	3.2	0.00
11	313	250	0.80	0.05129	2.23	0.24386	2.69	0.0345	1.51	221.6	5.4	218.5	3.2	0.03
12	339	275	0.81	0.04970	1.45	0.23730	2.09	0.0346	1.50	216.2	4.1	219.4	3.2	0.06
13	372	346	0.93	0.05158	1.45	0.24628	2.09	0.0346	1.50	223.5	4.2	219.4	3.2	0.05
14	295	279	0.95	0.04866	1.89	0.22961	2.42	0.0342	1.52	209.9	4.6	216.9	3.2	0.12
15	272	230	0.85	0.05185	1.77	0.24543	2.32	0.0343	1.50	222.9	4.6	217.6	3.2	0.04
X07-20 andesite														
1	393	690	1.76	0.05035	1.58	0.24177	2.18	0.0348	1.51	219.9	4.3	220.7	3.3	0.04
2	203	179	0.88	0.05285	2.18	0.24437	2.65	0.0335	1.50	222.0	5.3	212.6	3.1	0.00
3	536	644	1.20	0.04935	2.48	0.23911	2.91	0.0351	1.52	217.7	5.7	222.6	3.3	0.02
4	366	292	0.80	0.05197	1.64	0.24764	2.22	0.0346	1.51	224.7	4.5	219.0	3.2	0.03
5	293	332	1.13	0.04940	1.84	0.23637	2.38	0.0347	1.51	215.4	4.6	219.9	3.3	0.00
6	395	464	1.18	0.05142	1.59	0.24521	2.37	0.0350	1.51	222.7	4.8	222.1	3.3	0.09
7	462	550	1.19	0.05051	1.47	0.24495	2.10	0.0352	1.50	222.5	4.2	222.8	3.3	0.05
8	385	511	1.33	0.04835	1.66	0.22982	2.26	0.0345	1.54	210.1	4.3	218.5	3.3	0.07
9	436	677	1.55	0.05175	1.52	0.24652	2.14	0.0345	1.51	223.7	4.3	218.9	3.2	0.00
10	193	173	0.90	0.06163	2.60	0.23421	5.22	0.0341	1.51	213.7	10.1	216.1	3.2	1.93
11	251	223	0.89	0.05208	3.18	0.24105	3.51	0.0336	1.50	219.3	7.0	212.9	3.1	0.11
12	362	299	0.83	0.05221	1.69	0.24623	2.39	0.0347	1.50	223.5	4.8	220.0	3.2	0.10
13	392	373	0.95	0.05163	1.65	0.24083	2.43	0.0343	1.60	219.1	4.8	217.5	3.4	0.09
14	382	359	0.94	0.05086	1.67	0.24377	2.25	0.0348	1.51	221.5	4.5	220.3	3.3	0.07
15	329	347	1.06	0.04932	2.61	0.23392	3.02	0.0344	1.50	213.4	5.8	218.0	3.2	0.05
16	219	189	0.86	0.05135	2.21	0.24119	2.68	0.0341	1.51	219.4	5.3	215.9	3.2	0.00

Note: f_{206} is the percentage of common ^{206}Pb in total ^{206}Pb.

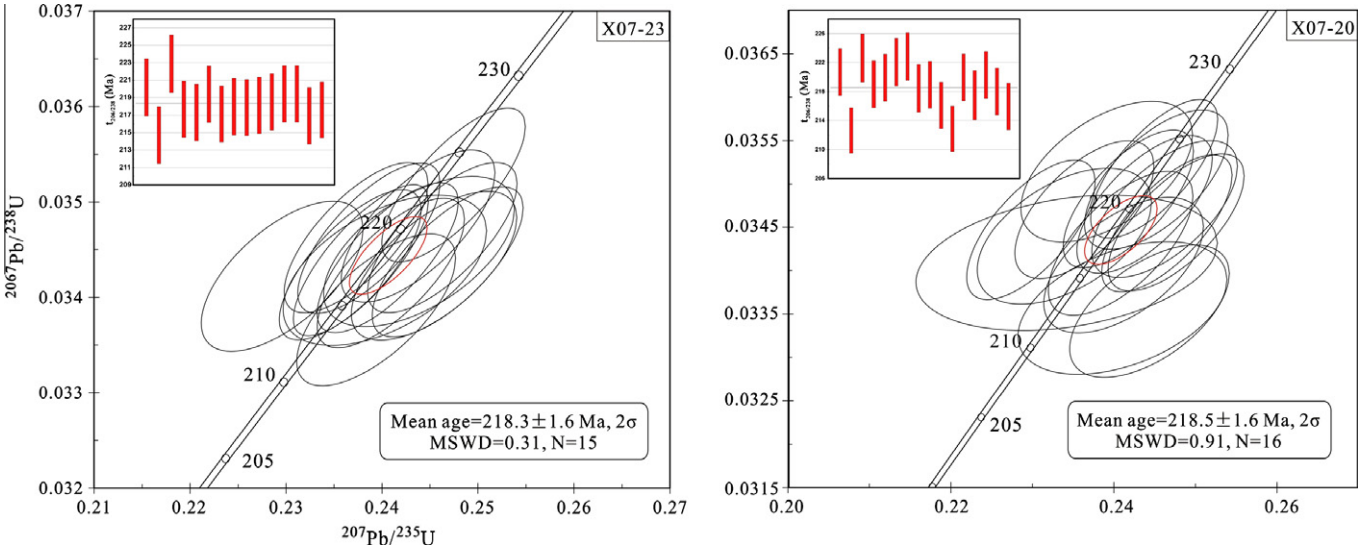

Fig. 8. U–Pb concordia plots for zircon grains from the sample X07-23 and X07-20 in the Xuejiping porphyry Cu deposit. The insets indicate the weighted mean $^{206}Pb/^{238}U$ ages.

have been adopted. These values were reported relative to the $^{176}Hf/^{177}Hf$ ratio of 0.282163 for the JMC475 standard. Single stage model ages (T_{DM1}) are calculated by using the measured $^{176}Lu/^{177}Hf$ ratios, referred to the $^{176}Hf/^{177}Hf$ ratio of 0.28325, which is similar to that of average MORB (Nowell et al., 1998) and the $^{176}Lu/^{177}Hf$ ratio of 0.0384 (Griffin et al., 2002) for a model of depleted mantle at present-day. This is similar, though not identical, to that of the depleted mantle curve defined by juvenile rocks through time (Vervoort and Blichert-Toft, 1999). Two-stage model ages (T_{DM2}) are calculated for the source rock of the magma under the assumption of a mean $^{176}Lu/^{177}Hf$ value of 0.015 for the average continental crust (Griffin et al., 2002).

4.4. Sr–Nd–Pb isotope analyses

The whole-rock Sr–Nd–Pb isotopic analysis was carried out by using an IsoProbe-T thermal ionization mass spectrometer (TIMS) at the Analytical Laboratory of the Beijing Research Institute

Table 4
Hf isotope analyses of samples X07-23 and X07-20.

Spots	$^{176}Yb/^{177}Hf$	±2σ	$^{176}Lu/^{177}Hf$	±2σ	$^{176}Hf/^{177}Hf$	±2σ	$t_{206/238}$ (Ma)	$\varepsilon_{Hf}(t)$	T_{DM1}(Ma)	T_{DM2}(Ga)
X07-23										
1	0.019308	0.000062	0.000813	0.000005	0.282666	0.000014	220	1.0	825	1.19
2	0.015906	0.000227	0.000680	0.000010	0.282686	0.000014	215	1.6	795	1.15
3	0.024040	0.000421	0.000957	0.000016	0.282659	0.000014	223	0.8	839	1.21
4	0.024451	0.000154	0.001013	0.000005	0.282704	0.000016	218	2.2	777	1.11
5	0.012814	0.000100	0.000540	0.000004	0.282674	0.000014	217	1.2	809	1.17
6	0.021818	0.000108	0.000938	0.000006	0.282675	0.000014	219	1.3	816	1.17
7	0.017602	0.000057	0.000734	0.000003	0.282678	0.000014	217	1.4	807	1.17
8	0.024704	0.000171	0.000967	0.000007	0.282669	0.000012	218	1.0	825	1.19
9	0.017182	0.000150	0.000712	0.000007	0.282672	0.000013	218	1.2	815	1.18
10	0.021089	0.000197	0.000846	0.000007	0.282650	0.000013	218	0.4	848	1.23
11	0.015130	0.000288	0.000659	0.000013	0.282690	0.000014	219	1.8	790	1.14
12	0.017547	0.000079	0.000718	0.000004	0.282662	0.000014	219	0.8	829	1.20
13	0.036531	0.000236	0.001472	0.000008	0.282660	0.000017	219	0.6	849	1.21
14	0.028675	0.000167	0.001150	0.000006	0.282682	0.000017	217	1.4	811	1.16
15	0.016774	0.000117	0.000696	0.000005	0.282671	0.000016	218	1.1	816	1.18
X07-20										
1	0.050695	0.000491	0.001838	0.000015	0.282677	0.000020	221	1.2	832	1.18
2	0.034696	0.000740	0.001304	0.000025	0.282714	0.000021	213	2.4	768	1.09
3	0.030074	0.000612	0.001105	0.000015	0.282686	0.000020	223	1.7	803	1.15
4	0.039473	0.000316	0.001496	0.000016	0.282658	0.000019	219	0.6	853	1.22
5	0.027837	0.000123	0.001084	0.000005	0.282692	0.000018	220	1.9	795	1.14
6	0.032903	0.000210	0.001281	0.000007	0.282679	0.000020	222	1.4	818	1.17
7	0.044788	0.000531	0.001658	0.000021	0.282645	0.000022	223	0.2	875	1.25
8	0.031779	0.000359	0.001240	0.000012	0.282700	0.000019	218	2.1	787	1.12
9	0.033119	0.000164	0.001242	0.000006	0.282663	0.000019	219	0.8	840	1.21
10	0.035173	0.000461	0.001316	0.000015	0.282666	0.000019	216	0.8	837	1.20
11	0.031273	0.000434	0.001160	0.000010	0.282735	0.000021	213	3.2	735	1.04
12	0.028405	0.000073	0.001156	0.000005	0.282704	0.000022	220	2.3	779	1.11
13	0.032269	0.000756	0.001248	0.000021	0.282684	0.000028	218	1.5	810	1.16
14	0.029410	0.000355	0.001196	0.000016	0.282699	0.000021	220	2.1	788	1.12
15	0.029776	0.000232	0.001203	0.000008	0.282705	0.000022	218	2.2	779	1.11
16	0.026442	0.000153	0.001062	0.000007	0.282638	0.000020	216	−0.2	871	1.26

Table 5
Whole-rock Sr and Nd isotopic compositions of altered porphyries and hosting andesite from the Xuejiping porphyry Cu deposit.

Lithology	Andesite		Diorite porphyry		Quartz monzonite porphyry		Quartz diorite porphyry	
Sample	XJP06-34	X07-20	X07-2	X07-21	XJP05-15	X07-23	X07-14	X07-15
Rb (ppm)	109	106	86.0	132	56.2	81.5	88.7	112
Sr (ppm)	1040	652	882	201	832	517	1177	637
Sm (ppm)	6.84	7.04	4.90	4.73	4.49	5.58	4.01	4.28
Nd (ppm)	37.4	37.8	28.9	27.7	24.8	33.7	24.4	26.5
$^{87}Rb/^{86}Sr$	0.3033	0.4704	0.2821	1.9066	0.1955	0.4561	0.2179	0.5088
$^{147}Sm/^{144}Nd$	0.1105	0.1125	0.1024	0.1032	0.1094	0.1000	0.0993	0.0979
$^{87}Sr/^{86}Sr$	0.706091	0.707118	0.706513	0.711277	0.706485	0.706717	0.706429	0.707493
±2σ (mean)	0.000010	0.000008	0.000011	0.000016	0.000007	0.000034	0.000008	0.000007
$^{143}Nd/^{144}Nd$	0.512368	0.512402	0.512306	0.512349	0.512377	0.512332	0.512389	0.512364
±2σ (mean)	0.000011	0.000012	0.000008	0.000007	0.000005	0.000008	0.000007	0.000008
$(^{87}Sr/^{86}Sr)_i$	0.70514	0.70565	0.70563	0.70531	0.70587	0.70529	0.70575	0.70590
$(^{143}Nd/^{144}Nd)_i$	0.512209	0.512240	0.512159	0.512200	0.512219	0.512188	0.512246	0.512223
$\varepsilon_{Nd}(t)$	−2.9	−2.2	−3.8	−3.0	−2.6	−3.3	−2.1	−2.6
T_{DM}(Ga)	1.15	1.13	1.15	1.10	1.13	1.10	1.01	1.03

Note: (1) $^{87}Rb/^{86}Sr$ and $^{147}Sm/^{144}Nd$ ratios are calculated using measured Rb, Sr, Sm and Nd contents. (2) $\varepsilon_{Nd}(t)$ values are calculated using present-day $(^{147}Sm/^{144}Nd)_{CHUR} = 0.1967$ and $(^{143}Nd/^{144}Nd)_{CHUR} = 0.512638$; T_{DM} values are calculated using present-day $(^{147}Sm/^{144}Nd)_{DM} = 0.2137$ and $(^{143}Nd/^{144}Nd)_{DM} = 0.51315$.

of Uranium Geology. The mass fractionation corrections for Sr and Nd isotopic ratios are undertaken on the basis of $^{86}Sr/^{88}Sr$ ratio of 0.1194 and $^{146}Nd/^{144}Nd$ ratio of 0.7219, respectively. The $^{87}Sr/^{86}Sr$ ratios of the NBS987 Sr standard and the $^{143}Nd/^{144}Nd$ ratio of the SHINESTU Nd standard applied in this study were 0.710250 ± 0.000007 (2σ) and 0.512118 ± 0.000003 (2σ), respectively. Pb was separated and purified by using a conventional cation-exchange technique (AG1 × 8, 200–400 resin) with diluted HBr used as eluant. The $^{208}Pb/^{206}Pb$, $^{207}Pb/^{206}Pb$ and $^{204}Pb/^{206}Pb$ ratios of the NBS981 Pb standard were 2.1681 ± 0.0008 (2σ), 0.91464 ± 0.00033 (2σ) and 0.059042 ± 0.000037 (2σ), respectively.

Rb, Sr, Sm, Nd, U, Th, and Pb contents are measured by ICP-MS at the State Key Laboratory of Ore Deposit Geochemistry (SKLODG), Institute of Geochemistry Chinese Academy of Sciences. The analytical procedures are described by Qi et al. (2000). The analytical precision is generally better than 10%.

5. Results

5.1. Molybdenite Re–Os ages

Re–Os data for five molybdenite samples from the Xuejiping deposit are listed in Table 2. Total Re concentrations are notably high,

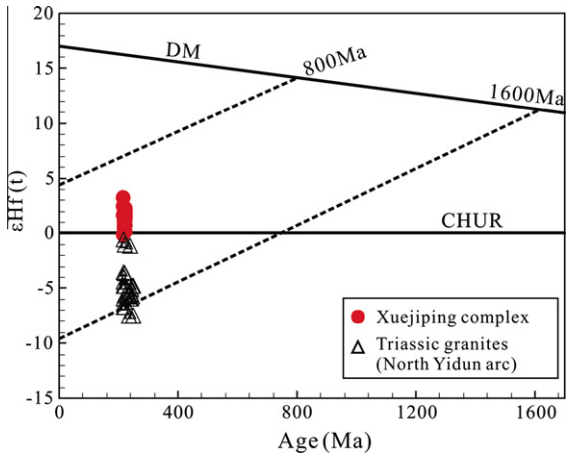

Fig. 9. Diagram of Hf isotopic evolution of zircon from the Xuejiping complex. The data of Triassic granites from north Yidun arc (triangle) are from Reid et al. (2007). The depleted mantle (DM) evolution is drawn by using $^{176}Hf/^{177}Hf$ ratio of 0.28325 and $^{176}Lu/^{177}Hf$ ratio of 0.0384 for DM at present (Griffin et al., 2000). The corresponding lines of crustal extraction are calculated by using the $^{176}Hf/^{177}Hf$ ratio of 0.015 for average continental crust (Griffin et al., 2002). CHUR, chondritic uniform reservoir.

varying from 728 to 2434 ppm. The ^{187}Os concentrations vary from 1.68 to 5.61 ppm. All the molybdenite Re–Os model ages vary in a relatively narrow range from 219.5 ± 1.5 Ma to 221.0 ± 2.1 Ma. They show an excellent reproducibility. An ^{187}Re-^{187}Os isochronal age of 221.4 ± 2.3 Ma (MSWD = 0.54) and a weighted mean age of 219.9 ± 0.7 Ma (MSWD = 0.88) have been obtained (Fig. 6). The interception on the ^{187}Os axis is nearly zero within uncertainty, with an initial ^{187}Os value of −0.015 ± 0.023 ppm (Fig. 6a). This is expected because molybdenite contains little or no non-radiogenic ^{187}Os. This indicates that the model age for molybdenite is reliable.

5.2. Zircon U–Pb ages

Zircon grains separated from the quartz monzonite porphyry (Sample X07-23) are mostly euhedral tetragonal dipyramids and tetragonal prisms (Fig. 7), with lengths varying from 100 μm to 300 μm and the length to width ratios varying from about 3:1 to 2:1. Igneous oscillatory zonation is clearly shown in all CL images of zircon grains. Fifteen U–Pb analyses of 15 zircon grains were obtained (Table 3). The concentrations of U and Th of these zircon grains vary from 184 ppm to 416 ppm and from 136 ppm to 457 ppm, respectively, with Th/U ratio varying from 0.65 to 1.09. All analyses are quite concordant within analytical errors (Fig. 8). Thus, a weighted mean $^{206}Pb/^{238}U$ age of 218.3 ± 1.6 Ma (MSWD = 0.31, 2σ) has been yielded. This age is interpreted as the crystallization age of the quartz monzonite porphyry.

Zircon grains separated from the andesite (Sample X07-20) are mostly euhedral to subhedral (Fig. 7). They are smaller (50–150 μm) than those of zircon grains separated from Sample X07-23. The CL images of these zircon grains show clear oscillatory zonation. 16 analyses show that concentrations of U and Th, and Th/U ratios of sixteen zircon grains (Table 3) vary from 193 ppm to 536 ppm, from 173 ppm to 677 ppm, and from 0.80 to 1.55, respectively. They are quite similar to those of the zircon grains separated from Sample X07-23. All analyses have yielded concordant U–Pb ages within analytical errors (Fig. 8), with a weighted mean $^{206}Pb/^{238}U$ age of 218.5 ± 1.6 Ma (MSWD = 0.91, 2σ), representing the formation age of andesite in the Tumugou Formation.

5.3. In situ zircon Hf isotopes

The U–Pb dated zircons from the above two samples were also analyzed for Lu–Hf isotopes on the same domains, and the results are listed in Table 4. As all zircon grains, which will be analyzed for Hf isotopes, show concordant U–Pb ages, little pre- or post-emplacement contamination to the zircon grains by non-radiogenic Hf could be occurred, hence the observed Hf ratios of the zircon grains could represent those of the parent melt (Stille and Steiger, 1991). The initial Hf ratios of the analyzed zircon grains were calculated on the basis of the previously measured $^{206}Pb/^{238}U$ age, respectively.

Fifteen analyses were made on 15 zircon grains from Sample X07-23. The calculated $\varepsilon_{Hf}(t)$ values vary positively from +0.4 to +2.2 with an average value of +1.2 (Table 4). Their corresponding single-stage Hf model ages (T_{DM1}) vary from 777 Ma to 849 Ma with an average of 820 Ma (Table 3). Similar $\varepsilon_{Hf}(t)$ values varying from −0.2 to +3.2 with an average of +1.5 have been yielded through sixteen analyses on 16 zircon grains from Sample X07-20. Their corresponding T_{DM1} model ages range from 735 Ma to 871 Ma with an average of 810 Ma.

5.4. Sr–Nd–Pb isotopic compositions

Eight samples including six altered porphyry samples and two peripheral andesite samples from the Tumugou Formation were selected for whole-rock Sr–Nd isotopes analysis. The results are given in Table 5. Based on the measured $^{87}Rb/^{86}Sr$ and $^{87}Sr/^{86}Sr$ ratios of all samples, an isochronal age of 206.7 ± 13.5 Ma (r = 0.9875)

Table 6
Whole-rock Pb isotopic compositions of the altered porphyries and peripheral andesite from the Xuejiping porphyry Cu deposit.

Lithology	Andesite		Diorite porphyry		Quartz monzonite porphyry		Quartz diorite porphyry
Sample	XJP05-33	XJP07-19	X07-2	X07-21	XJP05-15	XJP07-23	X07-14
U (ppm)	3.75	4.01	3.10	5.75	4.35	3.46	4.63
Th (ppm)	17.9	15.1	15.1	22.2	20	15.2	18.15
Pb (ppm)	28.7	20.7	25.79	30.70	41.6	485	23.87
$^{238}U/^{204}Pb$	8.26	12.30	7.74	11.87	6.59	0.45	12.30
$^{232}Th/^{204}Pb$	40.76	47.86	38.99	47.37	31.31	2.03	49.78
$^{208}Pb/^{204}Pb$	38.350	38.509	38.948	38.455	38.207	37.907	38.441
±2σ (mean)	0.001	0.004	0.005	0.005	0.002	0.002	0.005
$^{207}Pb/^{204}Pb$	15.578	15.589	15.640	15.559	15.551	15.530	15.559
±2σ (mean)	0.001	0.002	0.002	0.002	0.001	0.001	0.002
$^{206}Pb/^{204}Pb$	18.248	18.369	18.923	18.325	18.167	17.923	18.326
±2σ (mean)	0.001	0.002	0.003	0.002	0.001	0.001	0.003
$(^{208}Pb/^{204}Pb)t$	37.904	37.985	38.521	37.937	37.864	37.885	37.896
$(^{207}Pb/^{204}Pb)t$	15.564	15.567	15.626	15.538	15.539	15.529	15.537
$(^{206}Pb/^{204}Pb)t$	17.961	17.942	18.654	17.913	17.938	17.908	17.899

Note: $^{238}U/^{204}Pb$ and $^{232}Th/^{204}Pb$ ratios are calculated using whole-rock U, Th and Pb contents.

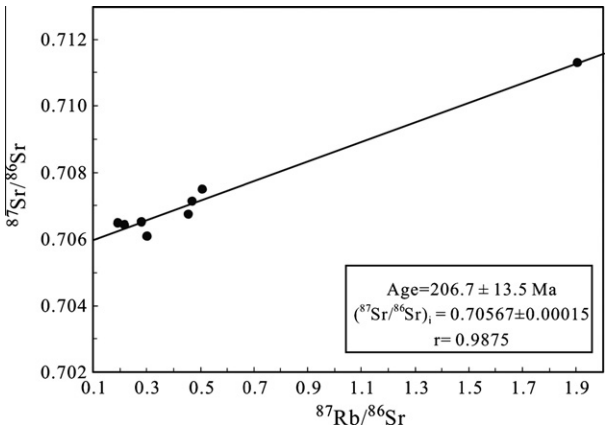

Fig. 10. Rb-Sr isochronal age and initial Sr isotopic composition for the Xuejiping complex.

and an initial $^{87}Sr/^{86}Sr$ ratio of 0.70567 ± 0.00015 have been yielded (Fig. 9). This isochronal age is quite consistent with the zircon U–Pb age within deviation. This indicates that the Rb–Sr isotopic system was not significantly disturbed by hydrothermal alteration. The initial $^{87}Sr/^{86}Sr$ and $\varepsilon_{Nd}(t)$ ratios are recalculated at the age of 220 Ma (zircon U–Pb ages). The calculated $(^{87}Sr/^{86}Sr)_i$ values, which range from 0.7051 to 0.7059 with an average of 0.7056, are in accordance with the $(^{87}Sr/^{86}Sr)_i$ value (0.70567 ± 0.00015) obtained through the Rb–Sr isochron. The calculated $\varepsilon_{Nd}(t)$ ratios vary from −3.8 to −2.1 with an average of −2.8, with the mantle-depletion Nd model ages (T_{DM}) varying from 1.01 Ga to 1.15 Ga.

Whole-rock Pb isotopic data indicate that both porphyry and andesite samples have similar Pb isotope compositions (Table 6). All samples are characterized by high radiogenic Pb isotopic compositions with the present-day whole-rock Pb isotopic ratios varying from 17.923 to 18.923 for $^{206}Pb/^{204}Pb$, from 15.530 to 15.64 for $^{207}Pb/^{204}Pb$ and from 37.907 to 38.948 for $^{208}Pb/^{204}Pb$, respectively. The initial Pb isotopic ratios were calculated at 220 Ma by using the single-stage Pb isotopic evolution model (Zartman and Doe, 1981). The calculated initial Pb isotope ratios vary from 17.899 to 18.654 for $(^{206}Pb/^{204}Pb)_t$, from 15.529 to 15.626 for $(^{207}Pb/^{204}Pb)_t$ and from 37.864 to 38.521 for $(^{208}Pb/^{204}Pb)_t$, respectively.

6. Discussion

6.1. Timing of the magmatism and mineralization

As mentioned above, previous isotopic dating results gave various ages for the Xuejiping ore-bearing porphyries. The obvious conflict between the hornblende $^{40}Ar–^{39}Ar$ plateau age of 249.3 ± 5.0 Ma by Zeng et al. (2003) and the zircon SHRIMP U–Pb ages of 215.3 ± 2.3 Ma by Lin et al. (2006) and 215.2 ± 1.9 Ma by Cao et al. (2009) indicate that the hornblende $^{40}Ar–^{39}Ar$ plateau age of 249.3 ± 5.0 Ma could not be reliable.

Our zircon SIMS U–Pb dating results show that the ore-bearing quartz monzonite porphyry and its host andesite have two precise and synchronous crystalline ages of 218.3 ± 1.6 Ma and 218.5 ± 1.6 Ma, respectively. They are a little bit older than those of ages obtained by Lin et al. (2006) and Cao et al. (2009).

The Xuejiping complex intruded into the strata of the Late Triassic Tumugou Formation which is determined by assemblage of fossils (e.g., *Halobia ganziensis Chen*, *superbesens, H.cf. yunnanensis*, *Palaeonucula stigilata*, *Cladiscites* sp., *Aulacoceras* sp., *Halobia* sp., *H.cf. austriaca, H.cf. yunnanensis, Posidoniasp., H. plicosa*, *H.cf. norica, Posidonia* sp., etc. YBGMR, 1990). Moreover, the ages of andesite in the Xuejiping area and basaltic andesite from the second member of Tumugou Formation in the Disuga area have been well confined to 218.5 ± 1.6 Ma and 219.8 ± 1.9 Ma, respectively (Leng, 2009). Therefore, the emplacement age of the ore-bearing porphyries from the Xuejiping deposit should not be older than the formation age of the Tumugou Formation. In this case, the hornblende $^{40}Ar–^{39}Ar$ plateau age of 249.3 Ma for the quartz diorite porphyry of the Xuejiping complex by Zeng et al. (2003) should be unreliable, whereas the previous published whole-rock Rb–Sr isochronal age (Tan et al., 1985) and the zircon U–Pb ages (Lin et al., 2006; Cao et al., 2009) should be acceptable.

The molybdenite Re–Os dating method has become a powerful tool to constrain the age of mineralization directly, due to the high Re and little common Os concentrations of molybdenite (Stein et al. 1997). In this study, Re–Os model ages varying from 219.5 Ma to 221.0 Ma with an isochronal age of 221.4 ± 2.3 Ma have been obtained by analyzing five molybdenite samples separated from Orebody IV. They are well in accordance with our zircon U–Pb ages of ore-bearing porphyries within deviation, but slightly older than previous zircon U–Pb ages of porphyries by Lin et al. (2006) and Cao et al. (2009). Therefore, it is suspected that the previous published zircon U–Pb ages could represent the timing of the

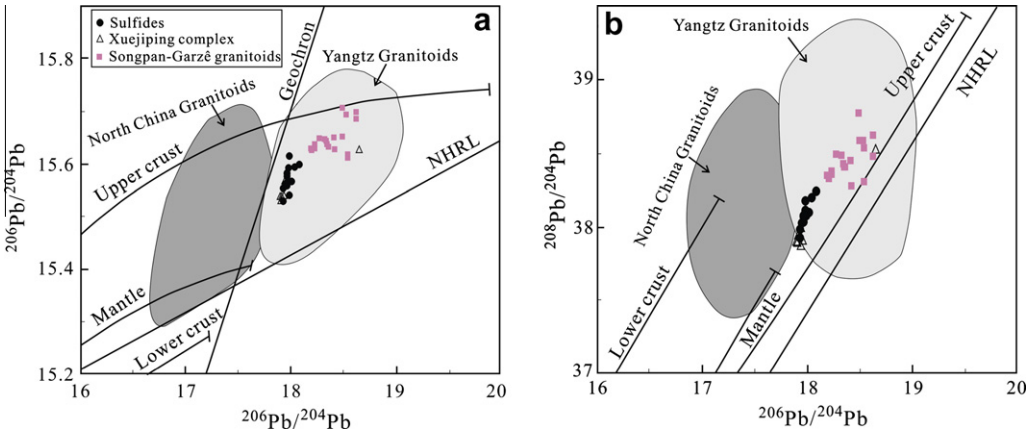

Fig. 11. (A) $^{207}Pb/^{206}Pb$ versus $^{206}Pb/^{204}Pb$ diagram; (B) $^{208}Pb/^{204}Pb$ versus $^{206}Pb/^{204}Pb$ diagram. Data of the North China and Yangtze granitoids are represented by K-feldspar Pb isotopic ratios of Mesozoic granitoids (Zhang, 1995). Data of Songpan-Garzê Mesozoic granitoids are from Zhang et al. (2006) and Xiao et al. (2007). Pb isotopic evolution lines of upper crust, lower crust and mantle are from Zartman and Doe (1981). NHRL, Northern Hemisphere reference line of Hart (1984).

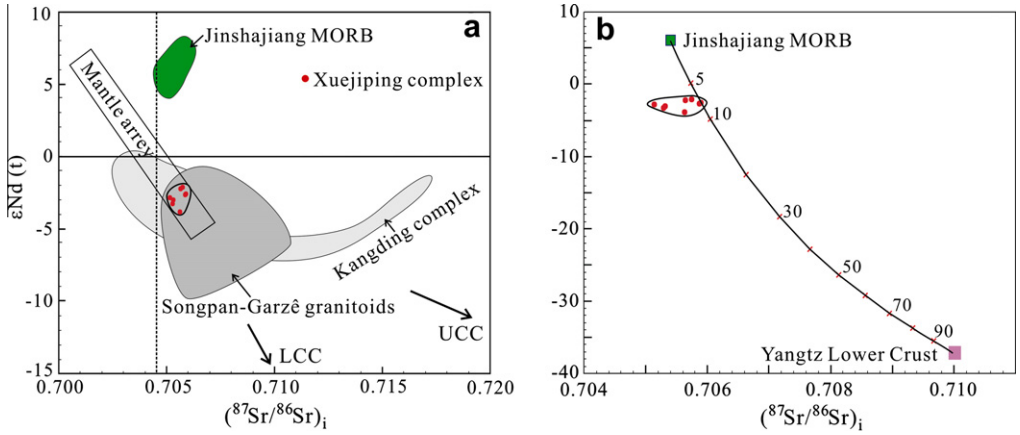

Fig. 12. (A) $\varepsilon_{Nd}(t)$ vs. $(^{87}Sr/^{86}Sr)_i$ diagram of the Xuejiping complex. All the initial isotopic ratios were corrected to 220 Ma. The trends of lower continental crust (LCC) and upper continental crust (UCC) are from Jahn et al. (1999). The data of Jinshajiang MORB are from Xu and Castillo (2004), the Songpan-Garzê granitoids from Zhang et al. (2006, 2007) and Xiao et al. (2007), and the Kangding Complex from Ling et al. (1998) and Chen and Yang (2006). (B) The simulated diagram of Sr–Nd isotopic mixing. The Jinshajiang MORB represents the mantle-drived end-member: $\varepsilon_{Nd}(t) = 6.1$, Nd = 7.2 ppm, $(^{87}Sr/^{86}Sr)_i = 0.7054$, Sr = 260 ppm (Xu and Castillo, 2004). Gneisses of the Yangtze Block LCC [$\varepsilon_{Nd}(t) = -37$, Nd = 21.9 ppm, $(^{87}Sr/^{86}Sr)_i = 0.710$, Sr = 380 ppm are estimated by Gao et al. (1999, 2011) and Ma et al. (2000). Figures on the mixing line refer to mass fractions (wt.%) of the crustal components in the mixed magmas.

post-mineral quartz diorite porphyry, rather than the syn-mineral porphyries.

6.2. Sources of magma

Because zircon is a resistant and refractory mineral during chemical weathering and partial melting, it is capable of preserving its primary Hf isotope composition of magma crystallization (Hanchar and Hoskin, 2003). The uniformity of initial Hf compositions (mostly between 0 and +2.0) of the ore-bearing quartz monzonite porphyry and andesite suggest that they could be originated from a cognate magma chamber. This view is also further confirmed by the Sr and Nd isotopic data of the porphyries and andesites. These positive $\varepsilon_{Hf}(t)$ values and relatively young T_{DM1} model ages (~0.8 Ga) of the porphyry and andesite from the Xuejiping deposit are significantly different from those of the Triassic granites from the north Yidun arc, due to their negative and variable $\varepsilon_{Hf}(t)$ values (varying from −1.0 to −7.5) and their old T_{DM1} model ages (~1.6 Ga) (Fig. 9) of the Triassic granites which are interpreted to derived from an isotopically heterogeneous crustal source (Reid et al., 2007). Both the positive $\varepsilon_{Hf}(t)$ values and relatively young T_{DM1} model ages suggest that mantle components could have played an important role on the magma evolution of porphyries and andesite in the Xuejiping area.

The radiogenic Nd and Sr isotopes have also been used as powerful tools to constrain the characteristics of the magma source and even locate fossil hydrothermal systems for porphyry copper deposits (e.g., Farmer and Depaolo, 1984, 1987; Lang and Titley, 1998; Cooke et al., 2007). The $(^{87}Sr/^{86}Sr)_i$ and $\varepsilon_{Nd}(t)$ values of the altered porphyries vary narrowly from 0.7053 to 0.7059 and from −3.8 to −2.1, respectively. They are well consistent with those of the fresh andesites from the Tumugou Formation (Table 4). As the $^{87}Rb/^{86}Sr$ and $^{87}Sr/^{86}Sr$ data of the altered porphyries and andesite samples could form a whole-rock isochronal age (Fig. 10), which is quite similar to the zircon U–Pb ages of the ore-bearing quartz monzonite porphyry and andesite, it is believed that the $^{87}Sr/^{86}Sr$ ratios of the altered porphyries were almost not disturbed by the hydrothermal alteration. Therefore, the Sr and Nd isotopic compositions can be used to trace the nature of the magma source.

The negative $\varepsilon_{Nd}(t)$ values and the relatively high values of $(^{87}Sr/^{86}Sr)_i$ ratios argue against the derivation of the parent magma from partial melting of depleted mantle or ancient crustal rocks. All the $\varepsilon_{Nd}(t)$ values and the $(^{87}Sr/^{86}Sr)_i$ ratios of all samples are plotted in the mantle array in the diagram of $\varepsilon_{Nd}(t)$ versus $(^{87}Sr/^{86}Sr)_i$ (Fig. 12a). They are similar to those of other oceanic island volcanic rocks in the world (e.g., Kerguelen), suggesting the possible mixing of two different end members (including depleted mantle and continental crustal rocks) (Zindler and Hart, 1986). The Jinshajiang MORB is used as the inferred depleted mantle component (Xu and Castillo, 2004), while the gneisses of the Yangtze lower crust (Gao et al., 1999, 2011; Ma et al., 2000) are taken as the continental crustal component, on the basis of following evidences. (1) Although the Archean-Proterozoic crystalline basement has not been identified within the Yidun arc, the Zhongza Massif was still thought to have been derived from the Yangtze Block because both the Zhongza Massif and the Yangtze Block have similar stratigraphic sequences and fossil assemblages (Chang, 1997; Reid et al., 2007). (2) Pb isotopic data of the altered porphyries and andesite provide another line of evidence that there is affinity between the Yangtze Block and the Yidun basement. (3) High initial Pb isotopic ratios of rocks from the Xuejiping deposit (Table 6; Fig. 11) are similar to those of the Yangtze Block, but are distinctly different to those of the North China Mesozoic granitoids (Zhang, 1995). Based on the two end-members, a mantle–crust mixing model is proposed here to evaluate the contribution of mantle to the formation of the Xuejiping porphyry complex (Fig. 12b). The estimated results show that 90–95% mantle sourced material mixing with 5–10% continental crust sourced material can explain the isotopic compositions of the altered porphyries and andesites from the Xuejiping deposit. This indicates that the parent magma of porphyry in the Xuejiping deposit could be derived dominantly from partial melting of mantle with contamination of minor crustal rocks.

6.3. Sources of ore-forming metals

Although factors controlling Re contents of molybdenite are still under debate (Berzina et al., 2005), several researchers emphasized that the metal source of the deposit was probably a key factor (e.g., Mao et al., 1999; Stein, 2006). Mao et al. (1999) suggested that the Re contents in molybdenite are decreased gradually from mantle to I-type and then to S-type granite-related deposits. Stein et al. (2001) also proposed that deposits involved mantle underplating or metasomatism, or melting of mafic and ultramafic rocks have significantly higher Re contents in associated molybdenite than

those deposits that are crustally derived. As noted above, the Xuejiping deposit shows a markedly high Re contents in the molybdenite (from 728 ppm to 2434 ppm, Table 2). These data resemble those in large subduction-related porphyry Cu–Mo–Au deposits (e.g., Zimmerman et al., 2003; Stein et al., 2004; Voudouris et al., 2009), but contrast sharply with much lower Re contents (tens of ppm to sub-ppm level) observed in the deposits that are crustally derived (e.g., Mao et al., 1999). Therefore, it is suggested that the high content of Re in molybdenite at the Xuejiping deposit is directly derived from partial melting of metasomatized mantle whereby Re is supplied by dehydration of the subducted Garzê-Litang oceanic crust.

A preliminary investigation of Pb and S isotopes for sulfides from the Xuejiping deposit has been conducted by Leng et al. (2008c). The measured $^{206}Pb/^{204}Pb$, $^{207}Pb/^{204}Pb$ and $^{208}Pb/^{204}Pb$ ratios of 14 sulfide samples including chalcopyrite, pyrite, galena and sphalerite vary from 17.929 to 18.082, from 15.528 to 15.614, and from 37.917 to 38.230, respectively. They are similar to those of the porphyries and andesites. This similarity suggests that Pb isotopes of both the Xuejiping complex and sulfides might have the same origin and similar evolution history.

The measured $\delta^{34}S$ values of 31 sulfide separates from the Xuejiping deposit range from −3.1‰ to +0.7‰ with an average of −1.1‰ and a tower distribution on the histogram of $\delta^{34}S$ (Leng et al., 2008c). They are roughly similar to that of the mantle-derived sulphur (0 ± 3‰, Chaussidon and Lorand, 1990), and are also consistent with those of other porphyry Cu deposits in the world (Rui et al., 1984; Ohmoto, 1986; Field et al., 2005). This indicates that the sulfur of the Xuejiping deposit was originated from a magmatic source.

6.4. Tectonic setting of the Xuejiping porphyry Cu deposit

It is generally accepted that the Yidun island arc has experienced an evolution history from the Indosinian subduction orogeny of oceanic crust (238–210 Ma), then the Yanshanian arc-continental collision orogeny (207–138 Ma) and post-orogenic extention (138–73 Ma), and then the Himalayan intra-continental strike–slip shearing (65–15 Ma) (Hou et al., 2001, 2003, 2004). Numerous Indosinian arc granitic bodies and coeval hypabyssal porphyry stocks and volcanic rocks are considered to be related to the westward-dipping subduction of the "Garzê-Litang Ocean" during Late Triassic. The tectonic framework, rock assemblages, and associated ore deposits between the northern and southern segments of the Yidun arc were obviously different. This is thought to have been resulted from the different subduction dip angle (Hou et al., 2004, 2007). The bimodal volcanic suites, in which VMS-type Cu–Zn–Pb deposits (e.g., Gacun) are hosted, are developed in the Changtai arc, which was characterized by intra-arc rifting, of the northern part of the Yidun arc. In contrast, there are abundant intermediate-felsic porphyries, in which porphyry and skarn type Cu polymetallic deposits are hosted, but there is lack of back-arc basin in the Zhongdian arc of the southern segment of the Yidun arc.

The Zhongdian arc has also experienced a complicated geodynamic evolution history (Yang et al., 2002). A range of mineral systems were developed in various evolution periods of the Zhongdian arc. A lot of magmatic-hydrothermal ore deposits including porphyry, skarn and epithermal types of Cu-polymetallic deposits are closely associated with Indosinian hypabyssal porphyry stocks in this area with over 10 Mt of contained Cu resources. Both the ages of magmatism and mineralization in the Xuejiping porphyry Cu deposit are similar to those of other porphyry deposits in the Zhongdian arc (e.g., Pulang, Lanitang, Chundu, etc.; Fig. 1b; Table 1). They are coincident with the period of the oceanic crust subduction orogeny in the Yidun arc (Hou et al., 2004). Therefore, it is believed that the Xuejiping porphyry Cu deposit was formed during the Late Triassic westward-dipping subduction of the Garzê-Litang oceanic crust.

6.5. Implications for exploration in the Xuejiping area

Comparing to other porphyry Cu (–Au–Mo) deposits in the world (Lowell and Guilbert, 1970; Corbett and Leach, 1998), the Xuejiping Cu deposit is characterized with a strong silicification and quartz–sericite–pyrite alteration, and a major stockwork veining mineralization in the quartz diorite porphyry body, but lacking of pervasive potassic alteration and dissemination mineralization. On the basis of following two evidences, it is proposed that the stockwork veining mineralization dominantly distributed in the phyllic zone could represent the upper part of the porphyry copper mineralization system, and there is possible potassic alteration zone and dissemination mineralization below the phyllic alteration zone.

(1) Abundant stockwork veins containing carbonate, pyrite, galena and sphalerite are observed in the phyllic and argillic zones in the Xuejiping area. They are usually presented at the top and outmost of the typical porphyry Cu mineralization system (Lowell and Guilbert, 1970). In addition, the large propylitic alteration zone is distributed within the diorite and andesite in the deposit area. This suggests that the depth of erosion after mineralization is very limited.
(2) Overwhelming majority of fluid inclusions in quartz veins or patches are aqueous inclusions (cf. Leng et al., 2008b; Zhang et al., 2009). The daughter mineral-bearing fluid inclusions are mainly observed in quartz patches but rarely observed in quartz stockwork veins. The lack of vapor-rich fluid inclusions in the quartz patches and veins from phyllic zone could indicate that the inclusion fluids were highly fractionated and trapped at relatively shallow level.

Some new porphyry-type Cu orebodies have been discovered recently in the Lannitang and Chundu deposits, which are close to the Xuejiping deposit, by Yunnan Huaxi Mining Co. Ltd. There could be more prospective Cu (Au) resources in depth of the Xuejiping district.

7. Conclusions

Following conclusions can be drawn from our combined studies on Re–Os dating of molybdenite, U–Pb dating and in situ Hf isotopes of zircons and the whole-rock Sr–Nd–Pb isotopes for the genesis of the Xuejiping porphyry copper deposit in the Zhongdian arc, Northwest Yunnan, China.

(1) Molybdenite Re–Os and zircon U–Pb dating results indicate that the Xuejiping porphyry Cu deposit was formed in Late Triassic and related to the subduction of the Garzê-Litang oceanic crust.
(2) The uniform and slight positive $\varepsilon_{Hf}(t)$ values, relatively young single-stage Hf model ages for zircons, in combination with the negative $\varepsilon_{Nd}(t)$ values and relative high $(^{87}Sr/^{86}Sr)_i$ ratios of porphyries and andesites, suggest that the Xuejiping intrusive complex was predominantly originated from the mantle with limited contamination of crustal materials (ca. 5–10%).
(3) The special geological and geochemical characters of the Xuejiping porphyry copper deposit comparing with other porphyry Cu deposits in the world indicates that there could be more prospective Cu resources in the depth of the Xuejiping district.

Acknowledgements

Without practical help and scientific cooperation of a number of laboratories and individuals, the research described in this paper could not have been completed. Thanks are due to Yali Sun for her help on molybdenite Re–Os dating, Xianhua Li, Qiuli Li, and Guoqiang Tang for their assistance on SIMS U–Pb dating, Hui Zhou for her help on zircon CL imaging, Jinhui Yang and Yueheng Yang for their help on Hf isotope analysis by using LA-ICP-MS, Jianyong Cui for his assistance on Nd–Sr–Pb isotopes analysis by using TIMS, and Chaozhi Yang for his field assistance. Many thanks are to Wei Terry Chen for his helpful suggestions and language improvement on earlier drafts of this paper. This study was jointly supported by Grants from the Natural Science Foundation of China (41003023), the Knowledge-innovation Program of the Chinese Academy Sciences (KZCX2-YW-Q04-01), the Natural Science Foundation of China (40873039), and the Special Fund of the State Key Laboratory of Ore Deposit Geochemistry. This manuscript also benefited greatly from reviews by James Mortensen, Ryan Mathur, and an anonymous reviewer. Bor-ming Jahn, Editor-in-Chief of JAES, is highly appreciated for his helpful suggestions.

References

Berzina, A.N., Sotnikov, V.I., Economou-Eliopoulos, M., Eliopoulos, D.G., 2005. Distribution of rhenium in molybdenite from porphyry Cu–Mo and Mo–Cu deposits of Russia (Siberia) and Mongolia. Ore Geology Reviews 26, 91–113.

Blichert-Toft, J., Albarede, F., 1997. The Lu–Hf geochemistry of chondrites and the evolution of the mantle–crust system. Earth and Planetary Science Letters 148, 243–258.

Burchfiel, B.C., Chen, Z., Liu, Y., Royden, L.H., 1995. Tectonics of the Longmen Shan and adjacent regions, central China. International Geology Review 37, 661–735.

Cao, D.H., 2007. Porphyry copper deposit model and exploration technique in Zhongdian, Yunan. A dissertation submitted to Chinese Academy of Geological Science for doctoral degree, 93 pp (in Chinese with English abstract).

Cao, D.H., Wang, A.J., Huang, Y.F., Zhang, W., Hou, K.J., Li, R.P., Li, Y.K., 2009. SHRIMP geochronology and Hf isotope composition of zircons from Xuejiping porphyry copper deposit, Yunnan Province. Acta Geologica Sinica 83, 1430–1435 (in Chinese with English abstract).

Chang, C., 1997. Geology and Tectonics of Qinghai–Xizang Plateau Solid Earth Sciences Research in China. Science Press, Beijing, 153 pp..

Chaussidon, M., Lorand, L.P., 1990. Sulphur isotope composition of orogenic spinel lherzolite massifs from Ariege (N.E. Pyrenees, France): an iron microprobe study. Geochimica et Cosmochimica Acta 54, 2835–2846.

Chen, B., Wang, K., Liu, W., Cai, Z., Zhang, Q., Peng, X., Qiu, Y., Zheng, Y., 1987. Geotectonics of the Nujiang–Lancangjiang–Jinshajiang Region. Geological Publishing House, Beijing, 204 pp (in Chinese).

Chu, N.C., Taylor, R.N., Chavagnac, V., Nesbitt, R.W., Boella, R.M., Milton, J.A., Germain, C.R., Bayon, G., Burton, K., 2002. Hf isotope ratio analysis using multi-collector inductively coupled plasma mass spectrometry: an evaluation of isobaric interference corrections. Journal of Analytical Atomic Spectrometry 17, 1567–1574.

Cooke, D.R., Wilson, A.J., House, M.J., Wolfe, R.C., Walshe, J.L., Lickfold, V., Crawford, A.J., 2007. Alkalic porphyry Au–Cu and associated mineral deposits of the Ordovician to Early Silurian Macquarie Arc, New South Wales'. Australian Journal of Earth Sciences 54, 445–463.

Corbett, G.J., Leach, T.M., 1998. Southwest Pacific Rim Gold–Copper Systems: Structure, Alteration, and Mineralization. Society of Economic Geologists, Special Publication, 237 pp.

De Bievre, P., Taylor, P.D.P., 1993. Table of the isotopic composition of the elements. International Journal of Mass Spectrometry Ion Processes 123, 149.

Fan, Y.H., Li, W.C., 2006. Geological characteristics of the Pulang porphyry copper deposit, Yunnan. Geology in China 33, 352–361 (in Chinese with English abstract).

Farmer, G.L., DePaolo, D.J., 1984. Origin of mesozoic and tertiary granite in the western United States and implications for pre-mesozoic crustal structure 2. Nd and Sr isotopic studies of unmineralized and Cu- and Mo-mineralized granite in the Precambrian Craton. Journal of Geophysical Research 89, 10141–10160.

Farmer, G.L., Depaolo, D.J., 1987. Nd and Sr isotope study of hydrothermally altered granite at San Manuel, Arizona: implications for element migration paths during the formation of porphyry copper ore deposits. Economic Geology 82, 1142–1151.

Field, C.W., Zhang, L., Dilles, J.H., Rye, R.O., Reed, M.H., 2005. Sulfur and oxygen isotopic record in sulfate and sulfide minerals of early, deep, pre-main stage porphyry Cu–Mo and late main stage base–metal mineral deposits, Butte district, Montana. Chemical Geology 215, 61–93.

Gao, S., Ling, W.L., Qiu, Y.M., Zhou, L., Hartmann, G., Simon, K., 1999. Contrasting geochemical and Sm–Nd isotopic compositions of Archean metasediments from the Kongling high-grade terrain of the Yangtze craton: evidence for cratonic evolution and redistribution of REE during crustal anatexis. Geochimica et Cosmochimica Acta 63, 2071–2088.

Gao, S., Yang, J., Zhou, L., Li, M., Hu, Z.C., Guo, J.L., Yuan, H.L., Gong, H.J., Xiao, G.Q., Wei, J.Q., 2011. Age and growth of the Archean Kongling Terrain, South China, with emphasis on 3.3 Ga granitoid gneisses. American Journal of Science 311, 153–182.

Grifin, W.L., Pearson, N.J., Belousova, E.A., Jackson, S.E., Achterbergh, E., O'Reilly, S.Y., Shee, S.R., 2000. The Hf isotope composition of cratonic mantle: LAM-MC-ICPMS analysis of zircon megacrysts in kimberlites. Geochimica et Cosmochimica Acta 64, 133–147.

Griffin, W.L., Wang, X., Jackson, S.E., Pearson, N.J., O'Reilly, S.Y., Xu, X., Zhou, X., 2002. Zircon chemistry and magma mixing, SE China: in-situ analysis of Hf isotopes, Tonglu and Pingtan igneous complexes. Lithos 61, 237–269.

Grifin, W.L., Pearson, N.J., Belousova, E.A., Saced, A., 2006. Comment: Hf-isotope heterogeneity in zircon 91500. Chemical Geology 233, 358–363.

Hanchar, J.M., Hoskin, P.W.O., 2003. Zircon. Reviews in Mineralogy and Geochemistry 53, 1–500.

Harrowfield, M.J., Wilson, C.J.L., 2005. Indosinian deformation of the Songpan Garze Fold Belt, northeast Tibetan Plateau. Journal of Structural Geology 27, 101–117.

Hart, S.R., 1984. A large-scale isotope anomaly in the Southern Hemisphere mantle. Nature 309, 753–757.

Hou, Z.Q., 1993. The tectono-magmatic evolution of Yidun island-arc and geodynamic setting of the formation of Kuroko-type massive sulphide deposits in Sanjiang region, southwestern China. Resource Geology 17, 336–350.

Hou, Z.Q., Mo, X., 1991. A tectono-magmatic evolution of Yidun island arc in Sanjiang region, China. Contribution to the Geology of the Qinghai-Xizang (Tibet) Plateau 21, 153–165 (in Chinese).

Hou, Z.Q., Mo, X.X., 1993. Geology, geochemistry and genetic aspects of kuroko-type volcanogenic massive sulphide deposits in Sanjiang region, southwestern China. Exploration and Mining Geology 2, 17–29.

Hou, Z.Q., Qu, X.M., Yang, Y.Q., 2001. Collision orogeny in the Yidun arc: evidence from granites in the Sanjiang region. China. Acta Geologica Sinica 75, 484–497 (in Chinese with English abstract).

Hou, Z.Q., Yang, Y.Q., Wang, H.P., Qu, X.M., Lü, Q.T., Huang, D.H., Wu, X.Z., Tang, S.H., Zhao, J.H., 2003. Collision-Orogenic Progress and Mineralization System of Yidun Arc. Geological Publishing House, Beijing, 345 pp. (in Chinese).

Hou, Z.Q., Yang, Y.Q., Qu, X.M., Huang, D.H., Lü, Q.T., Wang, H.P., Yu, J.J., Tang, S.H., 2004. Tectonic evolution and mineralization systems of the Yidun arc orogen in Sanjiang region, China. Acta Geologica Sinica 78 (1), 109–119 (in Chinese with English abstract).

Hou, Z.Q., Zaw, K., Pan, G.T., Mo, X.X., Xu, Q., Hu, Y.Z. and Li, X., Z, 2007. Sanjiang Tethyan metallogenesis in S.W. China: Tectonic setting, metallogenic epochs and deposit types. Ore Geology Reviews 31, 48–87.

Hou, Z.Q., Yang, Z.M., Qu, X.M., Meng, X.J., Li, Z.Q., Beaudoin, G., Rui, Z.Y., Gao, Y.F., Zaw, K., 2009. The Miocene Gangdese porphyry copper belt generated during post-collisional extension in the Tibetan Orogen. Ore Geology Reviews 36, 25–51.

Huang, C.K., Bai, Z., Zhu, Y.S., Wang, H.Z., Shang, X.Z., 2001. Copper Deposit of China. Geological Publishing House, Beijing, pp. 163–167 (in Chinese).

Iizuka, T., Hirata, T., 2005. Improvements of precision and accuracy in in-situ Hf isotope microanalysis of zircon using the laser ablation-MC-ICPMS technique. Chemical Geology 220, 121–137.

Jahn, B.M., Wu, F.Y., Lo, C.H., Tsai, C.H., 1999. Crust–mantle interaction induced by deep subduction of the continental crust: geochemical and Sr–Nd isotopic evidence from post-collisional mafic–ultramafic intrusions of the northern Dabie complex, central China. Chemical Geology 157, 119–146.

Lang, J.R., Titley, S.R., 1998. Isotopic and Geochemical characteristics of Laramide magmatic systems in Arizona and implications for the genesis of porphyry copper deposits. Economic Geology 93, 138–170.

Leng, C.B., 2009. Ore Deposit Geochemistry and Regional Geological Setting of the Xuejiping Porphyry Copper Deposit, Northwest Yunnan, China. A dissertation submitted to Graduate University of Chinese Academy of Sciences for Doctoral Degree. 161 pp (in Chinese with English abstract).

Leng, C.B., Zhang, X.C., Wang, S.X., Qin, C.J., Gou, T.Z., 2007. Geochemical characteristics of porphyry copper deposits in the Zhongdian area, Yunnan as exemplified by the Xuejiping and Pulang porphyry copper deposits. Acta Mineralogica Sinica 27, 414–422 (in Chinese with English abstract).

Leng, C.B., Zhang, X.C., Wang, S.X., Qin, C.J., Gou, T.Z., Wang, W.Q., 2008a. SHRIMP zircon U–Pb dating of the Songnuo ore-hosted porphyry, Zhongdian, Northwest Yunnan, China and its geological implication. Geotectonica et Metallogenia 32, 124–130 (in Chinese with English abstract).

Leng, C.B., Zhang, X.C., Qin, C.J., Wang, S.X., Ren, T., Wang, W.Q., 2008b. Study of fluid inclusions in quartz veinlets in the Xuejiping porphyry copper deposit, Northwest Yunnan, China. Acta Petrologica Sinica 24, 2017–2028 (in Chinese with English abstract).

Leng, C.B., Zhang, X.C., Wang, S.X., Wang, W.Q., Qin, C.J., Wu, K.W., Ren, T., 2008c. Sulfur and lead isotope compositions of the Xuejiping porphyry copper deposit in Northwest Yunnan, China: tracing for the source of metals. Journal of Mineralogy and Petrology 28, 80–88 (in Chinese with English abstract).

Li, W.C., 2007. The Tectonic Evolution of the Yidun Island Arc and the Metallogenic Model of the Pulang Porphyry Copper Deposit, Yunnan, SW China. A dissertation submitted to China University of Geosciences for Doctoral Degree. 109 pp (in Chinese with English abstract).

Li, X., Liu, W., Wang, Y., Zhu, Q., Du, D., Shen, G., Liu, C., Que, M., Yang, S., Li, D., Feng, Q., 1999. The Tectonic Evolution and Metallogenesis in the Tethys of the

Nujiang–Lancangjiang–Jinshajiang Area, south-western China. Geological Publishing House, Beijing, 276 pp (in Chinese).
Li, J.K., Li, W.C., Wang, D.H., Lu, Y.X., Yin, G.H., Xue, S.R., 2007. Re–Os dating for ore-forming event in the late of Yanshan Epoch and research of ore-forming regularity in Zhongdian Arc. Acta Petrologica Sinica 23, 2415–2422 (in Chinese with English abstract).
Li, X.H., Liu, Y., Li, Q.L., Guo, C.H., Chamberlain, K.R., 2009. Precise determination of Phanerozoic zircon Pb/Pb age by multicollector SIMS without external standardization. Geochemistry Geophysics Geosystems 10, Q04010. http://dx.doi.org/10.1029/2009GC002400.
Li, N., Chen, Y.J., Santosh, M., Yao, J.M., Sun, Y.L., Li, J., 2011. The 1.85 Ga Mo mineralization in the Xiong'er Terrane, China: implication for metallogeny associated with assembly of the Columbia supercontinent. Precambrian Research 186, 220–232.
Li, W.C., Zeng, P.S., Hou, Z.Q., White, N.C., 2011. The Pulang porphyry copper deposit and associated felsic intrusions in Yunnan Province, Southwest China. Economic Geology 106, 79–92.
Ling, H.F., Xu, S.J., Shen, W.Z., Wang, R.C., Lin, Y.P., 1998. Nd, Sr, Pb, O isotopic compositions of Late Proterozoic Gezong and Donggu granites in the west margin of Yangtz plate and comparison with other coeval granitoids. Acta Petrologica Sinica 14, 269–277 (in Chinese with English abstract).
Lin, Q.C., Xia, B., Zhang, Y.Q., 2006. Zircon SHRIMP U–Pb dating of the syn-collisional Xuejiping quartz diorite porphyrite in Zhongdian, Yunnan, China, and its geological implications. Geological Bulletin of China 25, 133–135, in Chinese with English abstract.
Lowell, J.D., Guilbert, J.M., 1970. Lateral and vertical alteration–mineralization zoning in porphyry ore deposits. Economic Geology 65, 373–408.
Ludwig, K.R., 2001. Users Manual for Isoplot/Ex (rev. 2.49): A Geochronological Toolkit for Microsoft Excel. Berkeley Geochronology Cenert., Special Publication, No. 1a, 55 pp.
Ma, C.Q., Ehlers, C., Xu, C.H., Li, Z.C., Yang, K.G., 2000. The roots of the Dabieshan ultrahigh-pressure metamorphic terrane: constraints from geochemistry and Nd–Sr isotope systematics. Precambrian Research 102, 279–301.
Mao, J.W., Zhang, Z.C., Zhang, Z.H., Du, A.D., 1999. Re–Os isotopic dating of molybdenites in the Xiaoliugou W (Mo) deposit in the northern Qilian mountains and its geological significance. Geochimica et Cosmochimica Acta 63, 1815–1818.
Mo, X.X., Lu, F.X., Shen, S.Y., Zhu, Q.W., Hou, Z.Q., 1993. Volcanism and metallogeny in the Sanjiang Tethys. Geological Publishing House, Beijing, 250 pp (in Chinese with English abstract).
Nowell, G.M., Kempton, P.D., Noble, S.R., Fitton, J.G., Sauders, A.D., Mahoney, J.J., Taylor, R.N., 1998. High precision Hf isotope measurements of MORB and OIB by thermal ionization mass spectrometry: insights into the depleted mantle. Chemical Geology 149, 211–233.
Ohmoto, H., 1986. Stable isotope geochemistry of ore deposits. In: Valley, J.W., Taylor, H.P., O'Neail, J.R. (Eds.), Stable Isotopes and high Temperature Geological Processes. Reviews in Mineralogy 16, 460–490.
Pan, G.T., Xu, Q., Hou, Z.Q., Wang, L.Q., Du, D.X., Mo, X.X., Li, D.M., Wang, M.J., Li, Z.X., Jiang, X.S., Hu, Y.Z., 2003. Archipelagic Orogenesis, Metallogenic Systems and Assessment of the Mineral Resources Along the Nujiang–Lancangjiang–Jinshajiang Area in Southwestern China. Geological Publishing House, Beijing, pp. 420 (in Chinese).
Qi, L., Hu, J., Gregoire, D.C., 2000. Determination of trace elements in grantes by inductively coupled plasma mass spectrometry. Talanta 51, 507–513.
Qu, X.M., Hou, Z.Q., Zhou, S.G., 2002. Geochemical and Nd, Sr isotopic study of the post-orogenic granites in the Yidun arc belt of northern Sanjiang region, southwestern China. Resource Geology 52, 163–172.
Ratschbacher, L., Frisch, W., Chen, C., Pan, G., 1996. Cenozoic deformation, rotation and stress patterns in eastern Tibet and western Sichuan, China. In: Yin, A., Harrison, M. (Eds.), The Tectonic Evolution of Asia. Cambridge University Press, Cambridge, pp. 227–249.
Reid, A.J., Wilson, C.J.L., Liu, S., 2005. Structural evidence for the Permo-Triassic tectonic evolution of the Yidun arc, eastern Tibetan Plateau. Journal of Structural Geology 27, 119–137.
Reid, A., Wilson, C.J.L., Liu, S., Pearson, N., Belousova, E., 2007. Mesozoic plutons of the Yidun arc, SW China: U/Pb geochronology and Hf isotopic signature. Ore Geology Reviews 31, 88–106.
Ren, S.K., Zhang, X.C., Yang, C.Z., 2001. Excusion guide Zhongdian porphyry Cu–Au district. Yunnan Gaoshan Exploration and Development Co Ltd, 33 pp.
Richards, J.P., 2003. Tectono-magmatic precursors for porphyry Cu–(Mo–Au) deposit formation. Economic Geology 98, 1515–1533.
Rollinson, H.R., 1993. Using Geochemical Data: Evaluation, Presentation, Interpretation. Longman, London, 352 pp..
Rui, Z.Y., Huang, C.K., Qi, G.M., Xu, J., Zhang, M.T., 1984. The Porphyry Cu (–Mo) Deposits in China. Geological Publishing House, Beijing, 350 pp. (in Chinese with English abstract).
Scherer, E., Munker, C., Mezger, K., 2001. Calibration of the lutetium–hafnium clock. Science 193, 683–687.
Sengör, A.M.C., 1985. Tectonic subdivisions and evolution of Asia. Technical University of Istanbul Bulletin 46, 355–435.
Sillitoe, R.H., 1972. A plate tectonic model for the origin of porphyry copper deposits. Economic Geology 67, 184–197.
Sláma, J., Košler, J., Condon, D.J., Crowley, J.L., Gerdes, A., Hanchar, J.M., Horstwood, M.S.A., Morris, G.A., Nasdala, L., Norberg, N., Schaltegger, U., Schoene, B., Tubrett, M.N., Whitehouse, M.J., 2008. Plešovice zircon—a new natural reference material for U-Pb and Hf isotopic microanalysis. Chemical Geology 249, 1–35.
Smoliar, M.I., Walker, R.J., Morgan, J.W., 1996. Re–Os ages of group IIA, IIIA, IVA, and IVB iron meteorites. Science 271, 1099–1102.
Stein, H.J., 2006. Low-rhenium molybdenite by metamorphism in northern Swed, recognition genesis global implications. Lithos 87, 300–327.
Stein, H.J., Markey, R.J., Morgan, J.W., Du, A., Sun, Y., 1997. Highly precise and accurate Re–Os ages for molybdenite from the East Qinling molybdenum belt, Shaanxi Province, China. Economic Geology 92, 827–835.
Stein, H.J., Markey, R.J., Morgan, J.W., Hannah, J.L., Schersten, A., 2001. The remarkable Re–Os chronometer in molybdenite: how and why it works. Terra Nova 13, 479–486.
Stein, H.J., Hannah, J.L., Zimmerman, A., Markey, R., Sarkar, S.C., Pal, A.B., 2004. A 2.5 Ga porphyry Cu–Mo–Au deposit at Malanjkhand, central India: implications for Late Archean continental assembly. Precambrian Research 134, 189–226.
Stille, P., Steiger, R.H., 1991. Hf isotope systematics in granitoids from the central and southern Alps. Contributions to Mineralogy and Petrology 107, 273–278.
Sun, Y.L., Xu, P., Li, J., He, K., Chu, Z.Y., Wang, C.Y., 2010. A pracrical method for determination of molybdenite Re–Os age by inductively coupled plasma-mass spectrometry combined with Carius tube-HNO_3 digestion. Analytical Methods 2, 575–581.
Tan, X.C., Zeng, Q.W., Su, W.N., 1985. Porphyry Deposits and Porphyry Copper Deposits in the East Part of West Yunnan: Kunming, Yunnan, Yunnan Institute of Geological Sciences, 140 pp. (unpublished report).
Tan, K.H., Li, G.J., Huang, D.Z., Zhang, S.Q., 2005. The ore-controlling conditions of large scale Pulang porphyry copper deposit. Yunan Geology 24, 167–174 (in Chinese with English abstract).
Vervoort, J.D., Blichert-Toft, J., 1999. Evolution of the depleted mantle: Hf isotope evidence from juvenile rocks through time. Geochimica et Cosmochimica Acta 63, 533–556.
Voudouris, P.C., Melfos, V., Spry, P.G., Bindi, L., Kartal, T., Arikas, K., 2009. Rhenium-rich molybdenite and rehniite in the Pagoni Rachi Mo–Cu–Te–Ag–Au prospect, northern Greece. implications for the Re geochemistry of porphyry-style Cu–Mo and Mo mineralization. The Canadian Mineralogist 47, 1013–1036.
Wang, E., Burchfiel, B.C., 2000. Late Cenozoic to Holocene deformation in southwestern Sichuan and adjacent Yunnan, China, and its role in formation of the southeastern part of the Tibetan Plateau. In: Geissman John, W., Glazner Allen, F. (Eds.), Special Focus on the Himalaya. Geological Society of America Bulletin, Boulder, CO, United States, pp. 13–423.
Wang, X., Metcalfe, I., Jian, P., He, L., Wang, C., 2000. The Jinshajiang–Ailoshan Suture Zone, China: tectonostratigraphy, age and evolution. Journal of Asian Earth Sciences 18, 675–690.
Wang, S.X., Zhang, X.C., Leng, C.B., Qin, C.J., 2007a. A tentative study of ore geochemistry and ore-forming mechanism of Pulang porphyry copper deposit in Zhongdian NW Yunnan. Mineral Deposits 26, 277–288 (in Chinese with English abstract).
Wang, S.X., Zhang, X.C., Qin, C.J., Shi, S.H., Leng, C.B., Chen, Y.J., 2007b. Fluid inclusions in quartz veins of the Pulang porphyry copper deposit, Zhongdian, northwestern Yunnan China. Geochimica 36, 467–4780 (in Chinese with English abstract).
Wang, S.X., Zhang, X.C., Leng, C.B., Qin, C.J., Ma, D.Y., Wang, W.Q., 2008a. Zircon SHRIMP U–Pb dating of the Pulang porphyry copper deposit, northwestern Yunnan, China: thee ore-forming time limitation and geological significance. Acta Petrologica Sinica 24, 2313–2321 (in Chinese with English abstract).
Wang, S.X., Zhang, X.C., Leng, C.B., Qin, C.J., Wang, W.Q., Zhao, M.C., 2008b. Stable isotopic compositions of the Hongshan skarn copper deposit in the Zhongdian area and its implication for the copper mineralization process. Acta Petrologica Sinica 24, 480–488 (in Chinese with English abstract).
Wang, B.Q., Zhou, M.F., Li, J.W., Yan, D.P., 2011. Late Triassic porphyritic intusions and associated volcanic rocks from the Shanggri-La region, Yidun terrane, Eastern Tibetan Plateau: adakitic magmatism and porphyry copper mineralization. Lithos 127, 24–38.
Woodhead, J.D., Hergt, J.M., 2005. A preliminary appraisal of seven natural zircon reference materials for in situ Hf-isotope analysis. Geostandards and Geoanalytical Research 29, 183–195.
Wu, F.Y., Yang, Y.H., Xie, L.W., Yang, J.H., Xu, P., 2006. Hf isotopic compositions of the standard zircons and baddeleyites used in U–Pb geochronology. Chemical Geology 234, 105–126.
Xiao, L., Zhang, H.F., Clemens, J.D., Wang, Q.W., Kan, Z.Z., Wang, K.M., Ni, P.Z., Liu, X.M., 2007. Late Triassic granitoids of the eastern margin of the Tibetan Plateau: geochronology, petrogenesis and implications for tectonic evolution. Lithos 96, 436–452.
Xu, J.F., Castillo, P.R., 2004. Geochemical and Nd–Pb isotopic characteristics of the Tethyan asthenosphere: implications for the origin of the Indian Ocean mantle domain. Tectonophysics 393, 9–27.
Xu, Z., Hou, L., Wang, Z., 1992. Orogenic Processes of the Songpan-Garzê Orogenic Belt of China. Geological Publishing House, Beijing, 190 pp. (in Chinese).
Xu, X.W., Chai, X.P., Qu, W.J., Song, B.C., Qin, K.Z., Zhang, B.L., 2006. Later Cretaceous granitic porphyritic Cu-Mo mineralization system in the Hongshan area, northwestern Yunnan and its significances for tectonics. Acta Geologica Sinica 80, 1422–1433 (in Chinese with English abstract).
Yang, Y.Q., Hou, Z.Q., Huang, D.H., Qu, X.M., 2002. Collision orogenic process and metallogenic system in Zhogndian arc. Acta Geoscientia Sinica 23, 17–24 (in Chinese with English abstract).
Yunnan Bureau of Geology and Mineral Resources (YBGMR), 1990. Regional Geology of Yunnan Province. Geological Publishing House, Beijing. 728 pp. (in Chinese).

Yin, A., Harrison, T.M., 2000. Geologic evolution of the Himalayan–Tibetan orogen. Annual Review of Earth and Planetary Science 28, 211–280.
Yin, G.H., Li, W.C., Jiang, C.X., Xu, D., Li, J.K., Yang, S.R., 2009. The evolution of Relin uplex rock masses in Yanshan phase and Ar–Ar dating age and copper-molybdenum mineralization characteristics of Zhongdian volcanic–magma arc. Geology and Exploration 45, 385–394 (in Chinese with English abstract).
Zartman, R.E., Doe, B.R., 1981. Plumbotectonics – the model. Tectonophysics 75, 135–162.
Zeng, P.S., Mo, X.X., Yu, X.H., Hou, Z.Q., Xu, Q.D., Wang, H.P., Li, H., Yang, C.Z., 2003. Porphyries and porphyry copper deposits in Zhongdian area, Northwest Yunnan. Mineral Deposits 20, 393–400 (in Chinese with English abstract).
Zeng, P.S., Hou, Z.Q., Li, L.H., Qu, W.J., Wang, H.P., Li, W.C., Memg, Y.F., Yang, Z.S., 2004. Age of the Pulang porphyry copper deposit in NW Yunnan and its geological significance. Geological Bulletin of China 23, 1127–1130 (in Chinese with English abstract).
Zeng, P.S., Li, W.C., Wang, H.P., Li, H., 2006. The Indosinian Pulang super large porphyry copper deposit in Yunnan, China: petrology and chronology. Acta Petrologica Sinica 22, 990–1000 (in Chinese with English abstract).
Zhang, L.G., 1995. Block-Geology of Eastern Asia Lithosphere-Isotope Geochemistry and Dynamics of Upper Mantle, Basement and Granite. Chinese Science Press, Beijing, 252 pp. (in Chinese with English abstract).
Zhang, N., Cao, Y., Lio, Y.A., Zhao, Y., Zhang, H., Hu, D., Zhang, R., Wang, L., 1998. Geology and metallogeny in the Garzê-Litang rift zone. Geological Publishing House, Beijing, 119 pp. (in Chinese).
Zhang, H.F., Zhang, L., Harris, N., Jin, L.L., Yuan, H.L., 2006. U–Pb zircon ages geochemical and isotopic compositions of granitoids in Songpan-Garzê fold belt, eastern Tibetan Plateau: constraints on petrogenesis and tectonic evolution of the basement. Contributions to Mineralogy and Petrology 152, 75–88.
Zhang, X.C., Leng, C.B., Qin, C.J., Wang S.S., Ren T., 2009. Geologic and fluid inclusion characteristics of the Xuejiping porphyry Cu deposit, Yunnan, China. Smart science for exploaration and mining. In: Proceedings of the 10th Biennial SGA Meeting of the Society for Geology Applied to Mineral Deposits, vol. 1, pp. 548–550.
Zhao, Z., 1995. Model of Indosinian porphyry Cu–Mo deposits in Zhongdian. Yunnan Geology 14, 342–348 (in Chinese).
Zhong, X.S., 1982. A primary study of geological characters and ore-forming factors of Xuejiping porphy cooper deposits. Yunnan Geology 1, 134–146 (in Chinese).
Zhong, D., 2000. Palaeotethysides in West Yunnan and Sichuan China. Solid Earth Science Researches in China. Science Press, Beijing, 248 pp.
Zhou, D., Graham, S.A., 1996. The Sonpan-Ganzi complex of the West Qinling Shan as a Triassic remnant ocean basin. In: Yin, A., Harrison, M. (Eds.), The Tectonic Evolution of Asia. Cambridge University Press, Cambridge, pp. 281–299.
Zimmerman, A., Stein, H., Markey, R., Fanger, L., Heinrich, C., von Quadt, A., Peytcheva, I., 2003. Re–Os ages for the elatsite Cu–Au deposit, Srednogorie zone, Bulgaria. In: Eliopoulos, D.G. et al. (Eds.), Mineral Exploration and Sustainable Development. Millpress, Rotterdam, pp. 1253–1256.
Zindler, A., Hart, S., 1986. Chemical geodynamics. Annual Review of Earth and Planetary Sciences 14, 493–571.